THESIS FOR THE DEGREE OF DOCTOR OF PHILOSOPHY

Development and Characterisation of Oxygen-Carrier Materials for Chemical-Looping Combustion

PAUL CHO

Department of Chemical and Biological Engineering
Environmental Inorganic Chemistry
Chalmers University of Technology
Göteborg, Sweden 2005

Development and Characterisation of Oxygen-Carrier Materials for Chemical-Looping Combustion

PAUL CHO
ISBN 91-7291-605-2

Doktorsavhandlingar vid Chalmers tekniska högskola
Ny serie nr 2287
ISSN 0346-718x

Department of Chemical and Biological Engineering
Environmental Inorganic Chemistry
Chalmers University of Technology

SE-412 96 Göteborg
Sweden

Telephone + 46 (0)31-772 1000

pcho@chalmers.se

Cover: The principal outline of Chemical-Looping Combustion, where the red sphere represent oxygen atom, brown; nitrogen, green; metal (for example a nickel atom), black; carbon, and blue; hydrogen, see chapter 1.1, page 2.

Cover printed by:
Chalmersbibliotekets reproservice
Göteborg, Sweden 2005

Development and Characterisation of Oxygen-Carrier Materials for Chemical-Looping Combustion

Paul Cho

Department of Chemical and Biological Engineering
Environmental Inorganic Chemistry
Chalmers University of Technology

ABSTRACT

For combustion with CO_2 capture, chemical-looping combustion (CLC) with inherent separation of CO_2 is a promising technology. Two interconnected fluidized beds are used as reactors. In the fuel reactor, a gaseous fuel is oxidized by an oxygen carrier, e.g. metal oxide particles, producing carbon dioxide and water. The reduced oxygen carrier is then transported to the air reactor, where it is oxidized by air back to its original form before it is returned to the fuel reactor.

The feasibility of using both natural iron ore and synthetic oxygen carriers based on oxides of iron, nickel, copper and manganese was determined. Oxygen carrier particles were produced by freeze granulation. They were sintered at 1300°C to 1600°C for 4 to 6 hours and sieved to a size range of 125 - 180 and 180 - 250 μm. To be able to study and compare the different types of oxygen carrier particles, a procedure for testing and evaluation was developed. The reactivity was evaluated in both fixed and fluidized bed laboratory reactors, simulating a CLC system by exposing the sample to alternating reducing and oxidizing conditions. In addition, the particles were characterized with respect to crushing strength, agglomeration, tendency for carbon deposition as well as chemical and physical parameters.

The rates of reaction varied and were highly dependent upon the oxygen carrier used. For the natural iron ore it was found that a high yield of CH_4 to CO_2 was possible although the solid reactivity was relatively low. The reactivity of the freeze granulated particles was considerably higher, with the oxygen carriers based on nickel and copper having the highest reactivity in comparison to Fe and Mn based particles. However all of the investigated samples had a reactivity sufficient for use in a CLC of interconnected fluidized beds. The copper oxide particles agglomerated and may not be suitable as an oxygen carrier.

For the nickel-based particles the formation of carbon was clearly correlated to low conversion of the fuel. For the real application of CLC process, the carbon formation should not be a problem, because the process should be run under conditions of high conversions of the fuel.

Iron oxide with aluminum oxide defluidized and agglomerated only after long reduction periods, in which significant reduction of the magnetite to wustite took place. This is an important observation, because reduction to wustite is not expected in chemical-looping combustion with high fuel conversion.

Keywords: Chemical-Looping Combustion, Oxygen Carrier, Carbon Dioxide Capture, CO_2 Separation, Carbon Formation, and Defluidization.

LIST OF PUBLICATIONS

This thesis is based on the work contained in the following papers, referred to by Roman numerals in the text:

I Mattisson T, Lyngfelt A, Cho P, 2001, *The use of iron oxide as oxygen carrier in chemical-looping combustion of methane with inherent separation of CO_2*. Fuel, *80*, 1953-1962.

II Cho P, Mattisson T, Lyngfelt A, 2002, *Reactivity of iron oxide with methane in a laboratory fluidized bed - application of chemical-looping combustion.* Proceedings of the 7th International Conference on Circulating Fluidized Beds, Niagara Falls, Ontario, Canada, 599-606.

III Cho P, Mattisson T, Lyngfelt A, 2004, *Comparison of iron-, nickel-, copper- and manganese-based oxygen carriers for chemical-looping combustion.* Fuel, *83*, 1215-1225.

IV Cho P, Mattisson T, Lyngfelt A, 2005, *Carbon Formation on Nickel and Iron Oxide-Containing Oxygen Carriers for Chemical-Looping Combustion.* Industrial and Engineering Chemistry Research, *44*, 668-676.

V Cho P, Mattisson T, Lyngfelt A, 2005, *Defluidization Conditions for Fluidized-Bed of Iron, Nickel, and Manganese oxide-Containing Oxygen-Carriers for Chemical-Looping Combustion,* Submitted for publication.

Table of Contents

Chapter 1

Introduction

Combustion of fossil fuels results in release of CO_2. It is generally accepted that a reduction in emissions of greenhouse gases like CO_2, which contribute to global climate change, is necessary. One of the possible options for achieving this is separation and sequestration of CO_2 from combustion. A number of known techniques can be used to carry out this separation, but a major disadvantage with most of these techniques is the large amount of energy that is required to obtain the CO_2 in pure form, which means that the efficiency of power plants decrease 7-12 percentage units. [Lyngfelt and Leckner, 1999] The major part of the total energy required for CO_2 capture and storage comes from the separation of CO_2, while typically one fourth of the energy is needed for the compression of the CO_2 to a liquid suitable for storage. The cost for the separation of CO_2 is significant which motivates efforts to develop methods with potentially low costs.

For combustion with CO_2 capture, chemical-looping combustion (CLC) with inherent separation of CO_2 is a promising technology. In CLC, a metal oxide is used as an oxygen carrier, which transfers oxygen from the combustion air to the fuel. [Richter and Knoche, 1983] Two interconnected fluidized beds are used as reactors. In the fuel reactor, a gaseous fuel is oxidized by an oxygen carrier, e.g. metal oxide particles, producing carbon dioxide and water. The reduced oxygen carrier is then transported to the air reactor, where it is oxidized by air back to its original state before it is returned to the fuel reactor. The main advantage with chemical-looping combustion compared to normal combustion is that CO_2 is inherently separated from the other flue gas components, i.e. N_2 and unused O_2, and thus costly equipment and efficiency losses for separation of CO_2 are avoided. [Ishida and Jin, 1994b and 1995]

The purpose of this work is to develop suitable oxygen carrier materials for the CLC process and to develop simple laboratory methods to compare such materials and assess the feasibility for industrial application. There are a number of properties that a suitable oxygen carrier should have, most important being sufficient reactivity and oxygen transfer capacity, high resistance to attrition and fragmentation and finally the particles should not agglomerate.

1.1 Chemical-Looping Combustion

The CLC system is composed of an air reactor and a fuel reactor, see *Figure 1.1*. Lyngfelt et al. proposed a design where these reactors were interconnected fluidized beds. [Lyngfelt et al., 2001] The gaseous fuel is introduced to the fuel reactor which contains an oxygen carrier which is reduced according to:

$$(2n+m)Me_xO_y + C_nH_{2m} \rightarrow (2n+m)Me_xO_{y-1} + nCO_2 + mH_2O \quad (1.1)$$

where Me_xO_y is the fully oxidized oxygen carrier and Me_xO_{y-1} is the reduced oxygen carrier. The flue gas stream leaving the fuel reactor contains nothing except CO_2 and H_2O if full oxidation of fuel has been achieved, which means that pure CO_2 can be obtained by cooling the gas and removing the water condensate.

The reduced oxygen carrier, Me_xO_{y-1} is then transported to the air reactor and oxidized by oxygen in the air according to:

$$Me_xO_{y-1} + 1/2O_2 \rightarrow Me_xO_y \quad (1.2)$$

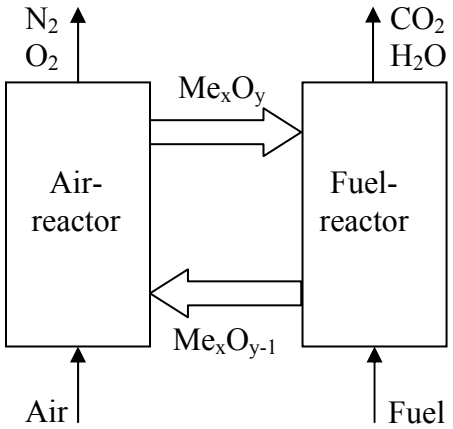

Figure 1.1 Chemical-looping combustion (CLC).

The flue gas stream leaving the air reactor contains N_2 and some remaining unused O_2. The oxidized oxygen carrier, Me_xO_y, is then transported back to the fuel reactor for another cycle. As a result, pure CO_2 can be inherently separated, thus potentially avoiding costs and energy consumption associated with a separation process. The total amount of heat released in reactions (*1.1*) and (*1.2*) is equal to the heat released from normal combustion.

1.2 Oxygen carriers

Important properties for oxygen carriers are high reactivity in both reduction by fuel gas and oxidation by oxygen in the air, as well as high resistance to attrition and fragmentation. Furthermore the oxygen carrier particles should not agglomerate. It is also an advantage if the oxygen carrier can be produced cheap and in an environmentally sound way. Some oxide systems of the transition metals, Fe, Cu, Co, Mn and Ni could be suitable as oxygen carriers. [Ishida et al., 1987, Richter and Knoche, 1983, Mattisson and Lyngfelt, 2001]

1.2.1 Thermodynamic and physical properties of oxygen carriers

Although it is possible to use gas from gasified coal as the fuel in CLC, fuels containing large amounts of methane, like natural gas or refinery gas, are more likely for a first application. The gas yield, γ_{red} *(equation 2.1)*, of CH_4 to CO_2 for the different oxide systems is shown in *Figure 1.2* for temperature intervals 900 to 1600 K.

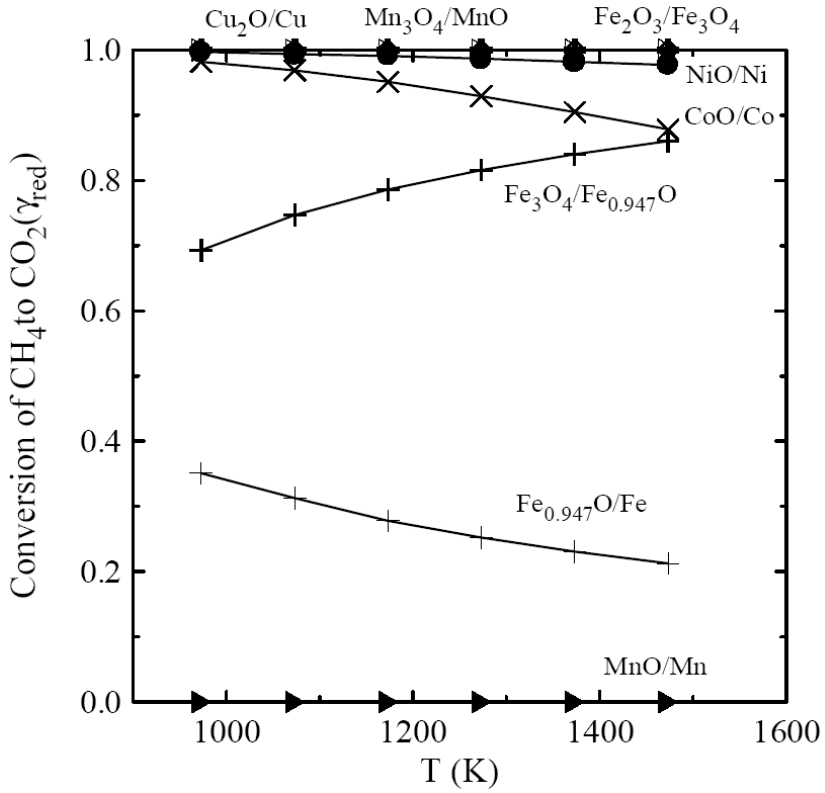

Figure 1.2 The gas yield, γ_{red}, of CH_4 to CO_2 vs. temperature for different metal oxide systems. Figure from Mattisson and Lyngfelt, 2001.

Table 1.1 Physical properties of selected metal and metal oxides. [Barin 1993a, b and Frenkel et al. 1994a, b.]

Chemical formula	Chemical name	Molecular weight (g/mole)	Solid density (g/mL)	Melting temperature (°C)
Fe_2O_3	Iron(III) oxide	159.7	5.2	1565
Fe_3O_4	Iron(II,III) oxide	231.5	5.2	1597
FeO	Iron(II) oxide	71.9	6.0	1377
Fe	Iron	55.9	7.9	1538
NiO	Nickel oxide	74.7	6.7	1955
Ni	Nickel	58.7	8.9	1455
Mn_2O_3	Manganese(III) Oxide	157.9	4.5	1347
Mn_3O_4	Manganese(II,III) Oxide	228.8	4.8	1562
MnO	Manganese(II) Oxide	70.9	5.4	1842
CuO	Copper(II) oxide	79.0	6.3	1446
Cu_2O	Copper(I) oxide	143.1	6.0	1235
Cu	Copper	63.6	9.0	1085

The conversion from CH_4 to CO_2 is complete for Cu_2O/Cu, Mn_3O_4/MnO and Fe_2O_3/Fe_3O_4 systems, and above 97% for the NiO/Ni system in the temperature range considered. As seen in *Figure 1.2* the further reduction of iron oxides to $Fe_{0.947}O$, or Fe, gives a lower conversion of the fuel and would most likely not be of interest for a process where high conversion of the fuel is desired.

Some oxides of higher oxidation state should also be mentioned. MnO_2 and Mn_2O_3 decompose in air at temperature above 460°C and 820°C, and to involve these oxides in the process would require even lower temperatures in the air reactor. Therefore these oxides are not expected to be of interest.

CuO is another oxide with high affinity for reaction with methane, which decomposes to Cu_2O in air at temperatures above 1030°C. The low melting temperature of Cu, 1085°C, in combination with experimental experiences of agglomeration suggest that particles with copper oxide would be used only at temperatures below 900°C. At these lower temperatures CuO can be expected to be formed in the air reactor, and therefore the copper oxide system most relevant for chemical looping combustion would be CuO/Cu. The physical properties of the selected metal and metal oxides are shown in *Table 1.1*.

In accordance with the thermodynamic considerations above, the relevant pairs of metal oxide/reduced metal oxide are CuO/Cu, NiO/Ni, Mn_3O_4/MnO, and Fe_2O_3/Fe_3O_4. The reaction enthalpies for these systems at 950°C with methane, carbon monoxide, and hydrogen are shown in the *Table 1.2*.

Table 1.2 Reaction enthalpies at 950°C. All reactions are normalized to 1 mol of O_2. Based on data from Barin 1993a, b and Frenkel et al. 1994a, b.

Reaction	ΔH (J/mole)	$\Delta H/\Delta H_{dir,comb,CH_4}$	$\Delta H/\Delta H_{dir,comb,CO}$	$\Delta H/\Delta H_{dir,comb,H_2}$
$O_2 + 1/2CH_4 \rightarrow 1/2CO_2 + H_2O$	-401183	1	-	-
$O_2 + 2CO \rightarrow 2CO_2$	-563235	-	1	-
$O_2 + 2H_2 \rightarrow 2H_2O$	-498311	-	-	1
$O_2 + 4Fe_3O_4 \rightarrow 6Fe_2O_3$	-481907	1.20	0.86	0.97
$O_2 + 2Ni \rightarrow 2NiO$	-468374	1.17	0.83	0.94
$O_2 + 2Cu \rightarrow 2CuO$	-297061	0.74	0.53	0.60
$O_2 + 6MnO \rightarrow 2Mn_3O_4$	-451361	1.13	0.80	0.91

The heat release in the air reactor can be compared to that of conventional combustion. In *Table 1.2*, ratios comparing the oxidation of the four metal oxides with oxidation of methane, carbon monoxide, and hydrogen are given. For instance, for oxidation of Ni, the heat release is increased by 17% compared to direct combustion of methane, and the corresponding amount of energy is absorbed by the endothermic reaction in the fuel reactor. Thus, the reaction in the fuel reactor is endothermic when this ratio is above 1, and exothermic when this ratio is below 1, cf. *Table 1.2*. It can be seen that the reaction in the fuel reactor is endothermic for reaction of methane with nickel, iron, and manganese oxide, whereas it is exothermic for reaction with copper oxide. In the case of both H_2 and CO, the reaction in the fuel reactor is exothermic for all these oxides.

1.2.2 Previous studies of oxygen carriers

There are a number of investigators of oxygen carrier for CLC. An overview of researchers from different parts of the world is presented below in alphabetic order of the nation, and a short summary of the experimental investigations is given in *Table 1.3*.

In the investigations below the reaction rates during oxidation and reduction varied in a wide range depending on the metal oxide and inert support used, but also depending on reaction conditions. In general, nickel, copper, and cobalt based carriers have a higher reduction reactivity compared to iron and manganese.

1.2.2.1 Italy

Villa and co-workers at Dipartimento di Chimica, Italy, investigated nickel based oxygen carriers with a thermogravimetric analyzer (TGA) using H_2 and CH_4 as fuel.

Table 1.3 Literature data on oxygen carriers for chemical-looping combustion

Reference	Oxygen carrier (Me_xO_y/support)	Reduction gas	T_{red} (°C)	D_p (mm)	Nation	Remarks
Nakano et al. 1986	Fe_2O_3, Fe_2O_3-Ni, Fe_2O_3/Al_2O_3	H_2, H_2O/H_2	700-900	0.007	Japan	
Ishida and Jin 1994a	NiO, NiO/YSZ, Fe_2O_3/YSZ	H_2	550, 750, 950	1.3, 2.0, 2.8	Japan	
Ishida et al. 1996	NiO/YSZ	H_2	600, 800, 1000	1.8, (1.0 - 3.2)[c]	Japan	
Ishida and Jin 1996	NiO, NiO/YSZ	H_2	600	2	Japan	a
Hatanaka et al. 1997	NiO	CH_4	400, 500, 600, 700	0.074	Japan	
Ishida and Jin 1997	NiO/YSZ, NiO/Al_2O_3, Fe_2O_3/YSZ,	CH_4, H_2O/CH_4	600, 700, 800	2	Japan	
Ishida et al. 1998	NiO/YSZ, NiO/Al_2O_3, NiO/TiO_2, Fe_2O_3/YSZ, Fe_2O_3/Al_2O_3, Fe_2O_3/TiO_2	H_2/N_2, CO/N_2, $CO/N_2/CO_2$, $CO/N_2/H_2O$	550, 600, 700, 800, 900	1.6	Japan	b
Jin et al. 1998	NiO/YSZ, Fe_2O_3/YSZ, CoO/YSZ, CoO-NiO/YSZ	H_2, CH_4	600	2	Japan	b
Jin et al. 1999	NiO/Al_2O_3, NiO/TiO_2, NiO/MgO CoO/Al_2O_3, CoO/TiO_2, CoO/MgO Fe_2O_3/ Al_2O_3, Fe_2O_3/ TiO_2, Fe_2O_3/MgO	H_2, H_2O/CH_4	600, 700	1.8	Japan	b, c
Copeland et al. 2000	CuO-based, Fe_2O_3-based	$H_2O/CO_2/H_2/CH_4$	800	Fine powder	USA	
Mattisson et al. 2000	Fe_2O_3, Fe_2O_3/ Al_2O_3, Fe_3O_4	CH_4	950	0.12-0.50	Sweden	
Copeland et al. 2001	Fe_2O_3-based, NiO-based	H_2/CH_4, Syngas	720-1000	-	USA	d
Jin and Ishida 2001	NiO, NiO/YSZ, NiO/Al_2O_3	H_2, H_2/Ar	600	1.8, 2.1, 4.0×1.5[e]	China, Japan	
Mattisson et al. 2001	Fe_2O_3 (iron ore)	CH_4	950	0.18-0.25	Sweden	
Ryu et al. 2001	NiO/bentonite, Ni/bentonite	CH_4/N_2	650, 700, 750, 800, 850, 900	0.080	South Korea	
Cho et al. 2002	Fe_2O_3/Al_2O_3, Fe_2O_3/MgO	CH_4	950	0.125-0.18, 0.18-0.25	Sweden	
Copeland et al. 2002	Fe_2O_3-based, NiO-based	Syngas	780	-	USA	d
Ishida et al. 2002	NiO/Al_2O_3	H_2, H_2/Ar	900	0.093	Japan	f
Jin and Ishida 2002	NiO/YSZ, NiO/Al_2O_3, CoO-NiO/YSZ	H_2O/CH_4	600, 700, 800	4.0×1.5[e]	China, Japan	b, c
Ryu et al. 2002	NiO/bentonite	CH_4/N_2	650, 700, 750, 800, 850, 900, 950, 1000	0.091	South Korea	b
Johansson 2002	NiO/TiO_2, Fe_2O_3/TiO2, CuO/ TiO_2, MnO_2/ TiO_2	CH_4, H_2O/CH_4	700, 725, 750, 800, 850, 900	1.5-2×2.5-3[g]	Sweden	
Jeong et al. 2003	$CoO_x/CoAl_2O_4$, NiO/$NiAl_2O_4$	H_2/Ar, CH_4/Ar/He	150-1000	-	South Korea	
Mattisson et al. 2003	NiO/Al_2O_3, CuO/Al_2O_3, CoO/Al_2O_3, Mn_3O_4/Al_2O_3	$H_2O/CO_2/N_2/CH_4$	750, 850, 950	0.1-0.5	Sweden	
Ryu et al. 2003	NiO/bentonite	CH_4/N_2	500, 600, 700, 800, 900, 1000	0.3-0.4	South Korea	b
Song et al. 2003	NiO/hexaaluminate	H_2/Ar	25 – 1000	-	South Korea	
Villa et al. 2003	NiO/$NiAl_2O_4$, $Ni_{1-y}Mg_yAl_2O_4$	H_2, CH_4/He	800, 25 – 1000	-	Italy	b
Adanez et al. 2004a	CuO, Fe_2O_3, MnO_2, NiO with Al_2O_3, sepiolite, SiO_2, TiO_2, ZrO_2	CH_4, H_2O/CH_4	800, 950	2×4[e]	Spain	
Adanez et al. 2004b	CuO, Fe_2O_3, MnO_2, NiO with Al_2O_3, SiO_2, TiO_2, ZrO_2	CH_4/N_2	800, 950	0.1-0.3	Spain	
Cho et al. 2004	Fe_2O_3/Al_2O_3, Fe_2O_3/Kaolin, NiO/$NiAl_2O_4$, CuO/$CuAl_2O_4$, Mn_3O_4 with $MnAl_2O_4$	CH_4/H_2O	850, 950	0.125-0.18	Sweden	
de Diego et al. 2004	CuO with Al_2O_3, sepiolite, SiO_2, TiO_2, ZrO_2	CH_4, H_2, or CO/H_2 in H_2O	800	0.2-0.4	Spain	

Reference	Oxygen carrier (Me_xO_y/support)	Reduction gas	T_{red} (°C)	D_p (mm)	Nation	Remarks
García-Labiano et al. 2004	CuO/Al_2O_3	CH_4/CO_2, CH_4/H_2O	800	0.1-0.3	Spain	
Johansson et al. 2004	$Fe_2O_3/MgAl_2O_4$	CH_4/H_2O	950	0.125-0.18	Sweden	
Lee et al. 2004	NiO with $AlPO_4$, ZrO_2, YSZ, $NiAl_2O_4$	H_2	600	-	South Korea	
Mattisson et al. 2004	Fe_2O_3 with Al_2O_3, ZrO_2, TiO_2, $MgAl_2O_4$	CH_4/H_2O	950	0.125-0.18	Sweden	
Ryu et al. 2004	NiO/bentonite	CH_4	750	0.106-0.212	South Korea	h
Brandvoll 2005	$NiO/NiAl_2O_4$, Perovskite[g]	H_2, CH_4, CH_4/H_2O	600, 700, 800	0.02-0.2 0.09-0.2 0.4-2.6	Norway	
Cho et al. 2005a	Fe_2O_3/Al_2O_3, $NiO/NiAl_2O_4$	CH_4, CH_4/H_2O	750, 850, 950	0.125-0.18	Sweden	b
Cho et al. 2005b	Fe_2O_3/Al_2O_3, $NiO/NiAl_2O_4$, $Mn_3O_4/Mg\text{-}ZiO_2$	CH_4	950	0.125-0.18	Sweden	i
Corbella et al. 2005	CuO/TiO_2	CH_4	800, 900	0.2-0.4	Spain	
Johansson et al. 2005	$NiO/MgAl_2O_4$	syngas or natural gas	850	0.09-0.212	Sweden	j
Lee et al. 2005	CoO/YSZ, NiO, NiO with ZrO_2, YSZ, $AlPO_4$, $NiAl_2O_4$	H_2	600	2	South Korea	
Lyngfelt and Thunman 2005	NiO based, Fe_2O_3 based	natural gas	750-900	-	Sweden	k
Mattisson et al. 2005	NiO with $NiAl_2O_4$, $MgAl_2O_4$, TiO_2, ZrO_2	CH_4/H_2O	950	0.125-0.18	Sweden	
Zafar et al. 2005	NiO, CuO, Mn_2O_3, Fe_2O_3 with SiO_2	CH_4/H_2O	800, 950	0.18-0.25	Sweden	

[a] No NO_x formation at 1200°C
[b] Study of carbon deposition
[c] Effect of pressure
[d] Spray dried particles.
[e] Cylindrical form, diameter×height
[f] Data from continuous CLC reactor
[g] $La_{0.8}Sr_{0.2}Co_{0.2}Fe_{0.8}O_3$
[h] 50 kW Chemical-Looping Combustor
[i] Study of defluidization
[j] 300 W laboratory reactor system
[k] 10 kW Chemical-Looping Combustor

1.2.2.2 Japan and China

The group of Ishida and co-workers at Tokyo Institute of Technology have conducted extensive amount of work concerning development of oxygen carriers for chemical-looping combustion. Nakano et al., performed the first experimental work in relation to CLC by investigating Fe_2O_3 with Al_2O_3 and Fe_2O_3 with Ni using a TGA. Since then Ishida, Jin and co-workers have investigated oxides of Fe, Ni, Co and Cu with Al_2O_3, yttria stabilized zirconia (YSZ), TiO_2 and MgO as support by using TGA with H_2 or CH_4 as fuel. Also work with fixed bed reactor and in continuous CLC reactor with gas chromatography (GC) has been presented.

Hatanaka and co-workers investigated NiO with CH_4 as fuel.

1.2.2.3 Norway

Bolland and co-workers investigated NiO with $NiAl_2O_4$ as support, as well as perovskite, in a batch reactor with either H_2, CH_4 or H_2O/CH_4 as fuel.

1.2.2.4 South Korea

Ryu and co-workers at Korea Institute of Energy Research investigated NiO with bentonite and hexaaluminate as support with TGA by using methane as fuel. Furthermore, CoO and NiO with ZrO_2, YSZ, $AlPO_4$, $NiAl_2O_4$ were investigated.

1.2.2.5 Spain

Adánez and co-workers at Instituto de Carboquímica (CSIC), investigated 240 extrudated types of oxygen-carrier particles, using oxides of copper, iron, manganese and nickel supported by either Al_2O_3, sepiolite, SiO_2, TiO_2 and ZrO_2 with a TGA using methane as fuel. Considerable work has also been performed on the behavior of impregnated particles of CuO in TGA and fixed bed reactors. Selected particles were investigated under fluidizing conditions as well.

1.2.2.6 Sweden

Mattisson and co-workers in Chalmers University of Technology have investigated both natural iron ore as well as freeze granulated and impregnated oxygen carriers in fixed bed, fluidized beds and thermogravimetric analyzers using methane as fuel. Oxides of the metals Fe,

Ni, Cu, Co and Mn have been used as the active material combined with inert supports of either Al_2O_3, $MgAl_2O_4$, SiO_2, ZrO_2, MgO, TiO_2 and kaolin. In some instances the active metal has reacted with the inert material to irreversible phases which has acted as the support material, for instance $NiAl_2O_4$. Oxygen carriers based on nickel and iron oxides were successfully tested with a 10 kW Chemical-looping combustor.

1.2.2.7 USA

Copeland and co-workers at TDA Research Inc. investigated oxygen carriers based on iron, copper and nickel, with H_2 and syngas as fuel.

1.3 Carbon formation

In chemical-looping combustion, i.e. in the reduction of metal oxide with methane in the fuel reactor, there may be side reactions which result in the formation of solid carbon on the particles. The conditions, for which carbon formation is thermodynamically possible, depend on the amount of oxygen added with the metal oxide as well as the temperature and pressure. In chemical-looping combustion, it could be important to avoid carbon formation during the oxidation of the fuel. The carbon may be transferred to the air reactor and oxidized to carbon dioxide, resulting in lower separation efficiency of carbon dioxide. It has also been suggested that it could have adverse effects on particles. [Ishida et al. 1998] Previous work has shown carbon formation on a number of iron- and nickel-based oxygen-carriers. The work however, was made under highly reducing conditions and the interpretation for a real application of chemical-looping combustion is not clear.

The carbon formation mechanisms have been studied in connection with synthesis gas production by partial oxidation of methane with suitable catalyst. There are two possible ways of carbon formation, either through methane decomposition,

$$CH_4 \rightarrow C + 2H_2 \tag{1.3}$$

or through the Boudouard reaction:

$$2CO \rightarrow C + CO_2 \tag{1.4}$$

Claridge and co-workers reported that a significant amount of carbon can be deposited on palladium and nickel catalysts. [Claridge et al., 1993] A mixture of methane/carbon monoxide,

pure methane or pure carbon monoxide was used as gas feedstock. Kinetically, both methane decomposition (*1.3*) and the Boudouard reaction (*1.4*) are known to be slow in the absence of a catalyst, but both reactions can be readily catalysed by many transition metals such as nickel and iron. They found that at higher temperature (above 617°C), the amount of carbon from pure carbon monoxide via the Boudouard reaction is very low compared with the amount deposited from methane decomposition and at lower temperature , i.e. 397°C, the Boudouard reaction (*1.4*) is favoured.

Ishida and co-workers investigated carbon deposition on oxygen-carrier particles based on nickel and iron oxide mixed with either yttria–stabilized zirconia (YSZ), Al_2O_3, or TiO_2 at 600°C using thermogravimetrical analysis (TGA). [Ishida et al., 1998] The particles were pre-reduced by a mixture of hydrogen and nitrogen gas and the carbon deposition was studied with a mixture of H_2O, carbon monoxide and nitrogen gas. The carbon deposition was indicated by increased weight of particle in TGA. They suggested that the carbon formation was caused by the Boudouard reaction (*1.4*), and found that the carbon deposition rates for iron-oxide based particles were lower than for nickel-oxide based particles except for the Fe_2O_3/YSZ particle. For nickel oxide, the binders affect the carbon deposition rate in the order of Al_2O_3 > YSZ > TiO_2. The effect of temperature on the carbon formation in the interval of 550 to 900°C was studied for the particle NiO/YSZ and showed that at 900°C, there was no carbon deposition. They found that the carbon deposits decreased with increased reaction temperature and H_2O/CO ratio.

Jin and co-workers investigated carbon depositions on oxygen-carrier particles based on nickel oxide mixed with either YSZ or $NiAl_2O_3$ at 600°C also using TGA, with either methane or humidified methane as fuel. [Jin et al., 1999] They found that the carbon deposition is mainly caused by methane decomposition (*1.3*) and that by addition of water vapor at the ratio of H_2O/CH_4 = 2.0, carbon deposition could be completely avoided on NiO/$NiAl_2O_3$. The carbon deposition on the oxygen-carrier particle CoO-NiO/YSZ at temperatures of 600, 700, and 800°C was also studied. [Jin and Ishida, 2002] They observed carbon deposition on particles at 700 and 800°C, if no water vapor was added. However, when water vapor was added, H_2O/CH_4 = 2.0, carbon formed only at 800°C.

Ryu and co-workers investigated the effects of different reaction temperatures on carbon deposition with an oxygen-carrier of NiO/bentonite using TGA. [Ryu et al., 2003] A mixture of methane and nitrogen was used as fuel and the investigated temperatures were in the range 650 to 1000°C. They showed that the carbon formation on the particle decreased with increased reaction temperature, and at temperatures above 900°C there was no carbon deposition. They found that at 900°C, carbon formation was seen when 90% or more of available oxygen in the metal oxide is consumed.

1.4 Defluidization

In chemical-looping combustion with fluidized beds a continuous circulation of oxygen carrier particles is necessary to transport the oxygen from air to the fuel. Thus it is important to avoid agglomeration of the particles which could lead to technical difficulties. Mattisson et al. reported tendency of agglomeration with iron based oxygen carriers and nickel oxide with titanium oxide as support. [Mattisson et al. 2004 and 2005] Lyngfelt and Thunman, and Johansson et al. reported tendency of agglomeration with iron based oxygen carriers. [Lyngfelt and Thunman, 2005 and Johansson et al. 2004] In previous works, the authors reported agglomeration tendencies on some of the iron oxide based oxygen-carriers [Cho et al., 2004] and showed that measurement of the pressure drop over the reactor gives good indication whether the bed of particles was fluidized or not. [Cho et al. 2005a] Thus, studies of defluidization were found to be useful to obtain better understanding of factors that influence agglomeration. Moreover, the latter study also suggested that there could be a connection between agglomeration and the length of the reducing period, i.e. the change in conversion. A possible consequence would be that the relevance of laboratory experiments for judging risks of agglomeration may be strongly dependent on the experimental conditions.

Chapter 2

Experimental section

2.1 Preparation of oxygen carrier

With the exception of particles of natural hematite (iron ore), freeze-granulation was used to produce the oxygen carriers studied. An overview and nomenclature of oxygen carriers used in this work is shown in *Table 2.1*. In freeze-granulation, commercial metal oxide powder and inert material, such as aluminum oxide powder were mixed with distilled water and with a small amount of dispersion agent. The mixture was then grinded in a ball mill for 17 h and the resulting slurry was made into frozen spherical particles by spraying the slurry through a nozzle into liquid nitrogen. The water in the frozen particles was then removed by freeze-drying. The particles were then heated to remove organic material and sintered at desired sintering temperature for 4 h, typically 1300°C. The heating rate was 2°C/min to 200°C, 1°C/min to 450°C, 10°C/min to desired sintering temperature. The oxygen carrier M4Z was sintered at 1150°C for 6 h and the heating rate was 2°C/min. The oxygen carriers were then sieved to different size ranges.

2.2 Determination of particle properties

The oxygen carriers were characterized before and after the experiments using X-ray powder diffraction (XRD, Siemens D5000 Powder Diffractometer utilizing Cu Kα radiation) and electron microscope (ESEM, Electroscan 2020). The force needed to crush the oxygen carriers was measured with digital force gauge (Shimpo FGN-5). The BET surface area and the porosity of the particles were measured with Gemini 2360 and AutoPore III mercury porosimeter (Micromeritics). The density of oxygen carrier particles was calculated assuming that the void was 0.37, corresponding to particles of spherical form and a loosely packed bed.

Table 2.1 Oxygen carriers used in this work.

Oxygen carrier	Active metal oxide, mass fraction in oxygen carrier	Support, mass fraction in oxygen carrier	Additive (%)	Particle diameter (μm)	Paper
Carajas[a]	Fe_2O_3	-	-	180-250	I
SYN7	Fe_2O_3, 60	Al_2O_3, 40	-	125-180, 180-250	II
SYN8	Fe_2O_3, 80	Al_2O_3, 20	-	125-180, 180-250	II
SYN9	Fe_2O_3, 40	Al_2O_3, 60	-	125-180, 180-250	II
SYN10	Fe_2O_3, 60	MgO, 40	-	125-180, 180-250	II
F6A	Fe_2O_3, 60	Al_2O_3, 40	-	125-180	III, IV, V
F6AS	Fe_2O_3, 60	Al_2O_3, 40	Starch, 10 volume % in slurry	125-180	III
F6K	Fe_2O_3 60	Kaolin, 40	-	125-180	III
F6KS	Fe_2O_3, 60	Kaolin, 40	Starch, 10 volume % in slurry	125-180	III
N6AN	NiO, 60	$NiAl_2O_4$, 40	-	125-180	III, IV
C6AC	CuO, 60	$CuAl_2O_4$, 40	-	125-180	III
M6AM	Mn_3O_4, 60	$MnAl_2O_4$, 40	-	125-180	III
N6AN1300	NiO, 60	$NiAl_2O_4$, 40	-	125-180	V
N6AN1400	NiO, 60	$NiAl_2O_4$, 40	-	125-180	V
N6AN1500	NiO, 60	$NiAl_2O_4$, 40	-	125-180	V
N6AN1600	NiO, 60	$NiAl_2O_4$, 40	-	125-180	V
M4Z	Mn_3O_4, 40	Mg-ZrO_2, 60	-	125-180	V

[a] Natural iron ore

2.3 Experimental setup and procedure

2.3.1 Experimental setup for fixed bed reactors

The tests of reactivity with natural hematite (iron ore) were carried out in two different fixed bed quartz reactors. Reactor I had a length of 860 mm with a porous quartz plate of 30 mm in diameter about 450 mm from the top. To reduce the residence time of the gas in the reactor, the top and bottom section was only 20 mm in diameter, while the middle section, where the iron oxide was placed on the quartz plate, was 30 mm in diameter. The temperature was measured using a 10% Pt/Rh thermocouple enclosed in a quartz shell 13 mm below the bottom of the quartz plate. A few experiments were performed in quartz reactor II. Reactor II was made in three different parts with a detachable middle section with a porous quartz plate 19 mm in diameter. This made it possible to weigh the sample accurately after the experiments. Because of the small volume of the middle reactor section, this reactor could only be used with small amounts of bed material. The experimental setup is shown in *Figure 2.1a.*

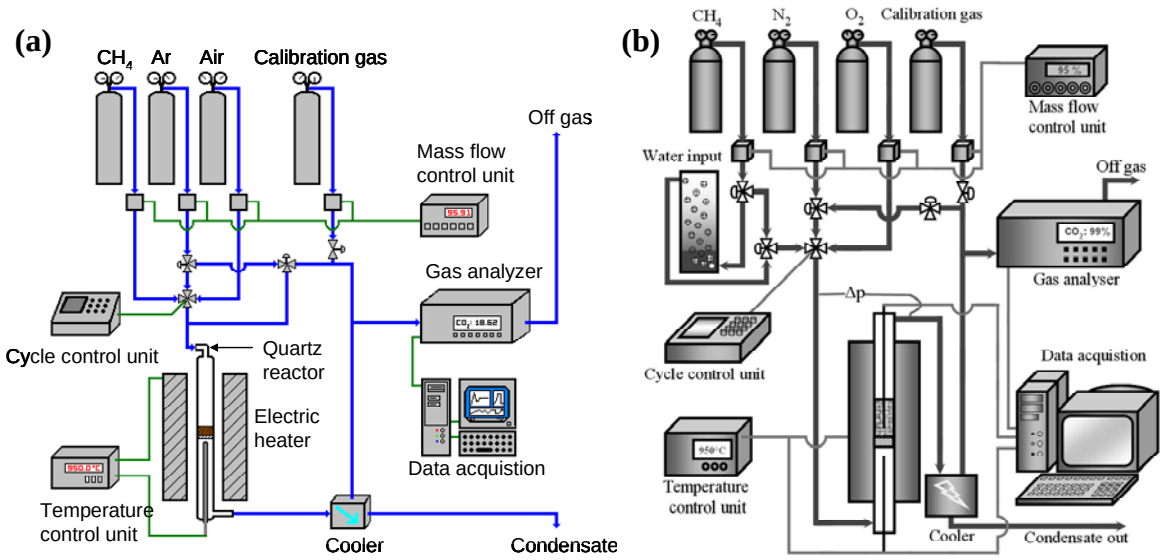

Figure 2.1 The experimental setup for (a) fixed bed and (b) fluidized bed.

2.3.2 Experimental setup for fluidized bed reactors

The experimental setup for the reactivity investigation with fluidized bed is shown in *Figure 2.1b*. The unit for addition of water vapor was only used in experiments reported in paper III and IV.

Several different types of quartz reactors were used for the fluidized bed experiments. Reactor I was used in the experiments reported in paper II. A third quartz reactor, reactor III, was used in experiments reported in paper III. This reactor had a length of 820 mm, with a porous quartz plate of 30 mm in diameter placed 370 mm from the bottom of the electric heater. The inner diameter of the bottom section was 19 mm and the top section was 30 mm.

The quartz reactor type IV was used in experiments reported in paper IV and V, and the quartz reactor type V is used in paper V. The quartz reactor type IV had a length of 820 mm, with a porous quartz plate of 20 mm in diameter placed 400 mm from the bottom of the quartz reactor. The inner diameter of the bottom section was 10 mm and the top section was 22 mm. The quartz reactor type V was conically shaped and had a length of 820 mm, with a porous quartz plate of 10 mm diameter placed 400 mm from the bottom of the quartz reactor. The inner diameter of the bottom section was 10 mm and the top section was 30 mm. The diameter increases from the quartz plate and 20 mm above the plate the full diameter, 30 mm, is reached.

The temperature of gas entering the bed was measured 5 mm under the porous quartz plate using a 10% Pt/Rh thermocouple enclosed in a quartz shell. The temperature of the fluidized bed

was measured 10 mm above the porous quarts plate, also with a 10% Pt/Rh thermocouple (reactor III, IV, V).

The pressure difference between inlet and outlet gas from the reactor was measured at 20 Hz with Honeywell pressure transducers (paper V).

2.3.3 Experimental procedure

In a typical experiment the oxygen carriers were first preheated in an inert atmosphere (Ar or N_2) to 950°C and then exposed to O_2 in air for 1000 s to ensure that the oxygen carriers were fully oxidized before the reduction period. The procedure is described in detail in paper I. During the reduction period, the oxygen carriers were then exposed to a gaseous fuel. In some experiments, H_2O was introduced during the reduction period to suppress possible carbon formation. The reduction period varied between 30 and 720 s. After the reduction period, an inert gas (Ar or N_2) was introduced for 120 to 200 s to avoid air and methane mixing during the shift between the reduction and the oxidation periods. The reduced oxygen carriers were then exposed to air or O_2 in nitrogen. This oxidation period varied between 400 and 3000 s. The lengths of the oxidation periods were chosen to ensure that full oxidation of the oxygen-carrier particles was attained. A full oxidation/reduction cycle consists of oxidation period, inert period, reduction period, and inert period. Typically, an experiment was conducted for between 6-40 oxidation/reduction cycles.

2.4 Data evaluation

The gas yield, γ_{red}, of methane to carbon dioxide was defined as:

$$\gamma_{\text{red}} = \frac{p_{\text{CO}_2,\text{out}}}{p_{\text{CH}_4,\text{out}} + p_{\text{CO}_2,\text{out}} + p_{\text{CO,out}}} \tag{2.1}$$

The conversion of oxygen carrier, X, or the degree of oxidation was defined as:

$$X = \frac{m - m_{\text{red}}}{m_{\text{ox}} - m_{\text{red}}} \tag{2.2}$$

The reduced form could be either the metal or a metal oxide with lower oxidation number than the oxidation number of fully oxidized metal oxide. Thus, the difference between m_{ox} and

m_{red} in equation (*2.2*) is the maximum theoretical amount of oxygen in the oxygen carrier which can be removed through oxidation of the fuel, here methane. The conversion of oxygen carrier, X, as function of time during the reduction period can be calculated from the outlet gas concentrations by;

$$X = 1 - \int_{t_0}^{t_1} \frac{\dot{n}_{out}}{n_O p_{tot}} \left(4 p_{CO_2,out} + 3 p_{CO,out} - p_{H_2,out}\right) dt \tag{2.3}$$

where t_0 is the time when the reduction started, and t_1 is when the inert period started.

The partial pressure of H_2 was estimated using the relation (*2.4*), by assuming equilibrium of H_2, H_2O, CO and CO_2 in the shift reaction (*2.5*);

$$p_{H_2,out} = \frac{2Kp_{CO,out}(p_{CO_2,out} + p_{CO,out})}{p_{CO_2,out} + Kp_{CO,out}} \tag{2.4}$$

where K, the equilibrium constant for reaction (2.4), is 0.67 at 950°C, 0.89 at 850°C, and 1.28 at 750°C.

$$CO + H_2O \rightarrow CO_2 + H_2 \tag{2.5}$$

The conversion of oxygen carrier, X, as function of time during the oxidation period was defined as;

$$X = X_0 + \int_{t_2}^{t_4} \frac{2}{n_O p_{tot}} \left(\dot{n}_{in} p_{O_2,in} - \dot{n}_{out} p_{O_2,out}\right) dt \tag{2.6}$$

where X_0 is the conversion at the start of the oxidation period, t_2 is the time when the oxidation started, t_4 is when the oxidation period ended.

Because different oxygen carriers can transfer different amounts of oxygen per mass unit it is an advantage to be able to compare them using a mass-based conversion. In this work, a mass-conversion was defined as,

$$\omega = \frac{m}{m_{ox}} = 1 - R_O(1 - X) \tag{2.7}$$

where R_O is the oxygen ratio and defined as:

$$R_O = \frac{(m_{ox} - m_{red})}{m_{ox}} \tag{2.8}$$

The oxygen ratio indicates the maximum mass flow of oxygen that can be transferred between the air and fuel reactor in CLC for a given mass flow of recirculating particles. The mass-based conversion rate, $d\omega/dt$, was calculated as:

$$\frac{d\omega}{dt} = R_O \frac{dX}{dt} \tag{2.9}$$

If the mass transfer resistance between bubbles and emulsion phase in the fluidized bed is negligible and the reaction is first order with respect to methane, the oxygen carrier will be exposed to a log-mean partial pressure of methane, $p_{CH_4,lgmean}$, defined as;

$$p_{CH_4,lgmean} = \frac{(p_{CH_4,in} - p_{CH_4,out})}{\ln(p_{CH_4,in} / p_{CH_4,out})} \tag{2.10}$$

and an effective reaction rate constant, $k_{\omega,eff}$, can be defined:

$$k_{\omega,eff} = \frac{(d\omega/dt)}{p_{CH_4,lgmean}} \tag{2.11}$$

Note that $k_{\omega,eff}$ is a function of the conversion, ω,. For a limited range in ω, e.g. $\Delta\omega$=0.01, where the variation in $k_{\omega,eff}$ is moderate, the effective rate constant can be approximated by an average value.

A normalized mass-based conversion rate, $(d\omega/dt)_{norm}$, can be defined using a chosen partial pressure of methane, p_{ref}:

$$\left(\frac{d\omega}{dt}\right)_{norm} = k_{\omega,eff}\ p_{ref} \tag{2.12}$$

To facilitate a comparison of reaction rates between different oxygen carriers a rate index, *RI* was defined as:

$$RI = 100 \cdot 60 \cdot \left(\frac{d\omega}{dt} \right)_{norm} \tag{2.13}$$

Thus, the rate index, *RI*, is the normalized mass-based conversion rate expressed in %/min.

If mass transfer resistance is assumed to be small, an estimate of the mass of oxygen carrier needed in a reactor, m_{bed}, can be made from the normalized mass-based conversion rate:

$$m_{\text{bed}} = \frac{\omega \dot{m}_{\text{O}}}{(d\omega/dt)_{\text{norm}}} \tag{2.14}$$

where $\dot{m}_{\text{O}}$ is the stoichiometric mass flow of oxygen to be transferred between two reactors.

If the fuel is assumed to be methane, $\dot{m}_{\text{O}}$ is obtained as,

$$\dot{m}_{\text{O}} = M_{\text{O}_2} \frac{\left(P_{\text{th}}/H_{\text{CH}_4}\right)}{M_{\text{CH}_4}} S_{\text{r}} \tag{2.15}$$

The oxygen carrier recirculation rate between the air and fuel reactor, $\dot{m}_{\text{sol}}$, is:

$$\dot{m}_{\text{sol}} = \frac{\omega_{\text{air}} \dot{m}_{\text{O}}}{\Delta\omega} \tag{2.16}$$

The carbon formation during the reduction period is calculated by integrating the total amounts of carbon dioxide and carbon monoxide produced during the subsequent inert and oxidation period. The carbon formation ratio, C/C_{tot}, is the amount of carbon formed during the reduction period over the total amount of carbon introduced during the reduction period and defined as;

$$\frac{C}{C_{tot}} = \frac{\int_{t_1}^{t_3} \dot{n}_{\text{out}} \left(p_{\text{CO}_2,\text{out}} + p_{\text{CO,out}} \right) dt}{\int_{t_0}^{t_3} \dot{n}_{\text{out}} \left(p_{\text{CH}_4,\text{out}} + p_{\text{CO}_2,\text{out}} + p_{\text{CO,out}} \right) dt} \tag{2.17}$$

where t_3 is a point of time in the oxidation period when no more carbon dioxide or carbon monoxide was registered.

Chapter 3

Results

The investigation of suitable oxygen carrier for CLC started in a fixed bed reactor with natural iron ore (paper I). Iron ore was chosen as a first material to study because it is safe, cheap and available in large quantities. To better simulate the actual conditions which an oxygen carrier is exposed to in a CLC combustor, a new experimental setup using a fluidized bed was developed. Furthermore, new oxygen-carrier particles made by freeze granulation were tested (paper II). The use of both fixed and fluidized bed reactors give a way of estimating the reactivity of oxygen carriers as well as the gaseous reaction products. The tests in the fluidized bed provide the additional advantage of establishing whether the particles can fluidize under reducing and oxidizing conditions, something which is important for a real process. The tests were combined with crushing strength tests to obtain an indication of the resistance to attrition/fragmentation.

The reactivity tests presented in Paper I and II were made with differing amounts of bed material, and the reactivity was presented in the form of an average conversion rate as function of the gas conversion attained as well as the total change in conversion. However, this means that several tests are needed for each particle, and in addition the comparison between different particles becomes complex. In order to compare a larger number of particles a standardized reactivity test procedure was developed (paper III). This was combined with an evaluation procedure leading to a single number that gives an indication of the reactivity, i.e. a rate index. Thus, it is possible to show reactivity versus particle strength and agglomeration tendency, which facilitates comparison of different oxygen carrier materials. This rate index is also useful for a technical evaluation of the process since it is inversely proportional to the estimated amount of bed material needed.

Previous extensive studies concerning carbon deposition on oxygen-carrier have been made using TGA and high concentration of reducing gas. In this study (paper IV) the carbon formation was investigated as function of the conversion of the fuel and oxygen carrier in order to assess if it could be a problem in a real process where high conversion of fuel is needed. From the outlet gas concentrations of carbon dioxide and carbon monoxide during the inert and oxidation period,

the carbon formation on oxygen-carrier particles during the reduction period was obtained. With this approach the carbon formed also during high methane conversion may be detected.

The study of defluidization (paper V) of oxygen-carrier particle have been made to give better understanding the connection between agglomeration and the length of the reducing period, i.e. the change in conversion.

3.1 Fixed bed reactor experiments with iron ore (paper I)

For all of the experiments where the reduction was investigated, the outlet concentration of CH_4, CO, CO_2 and O_2 showed similar behavior as the experiment with iron ore shown in *Figure 3.1a and b*. In general, during the reduction period the majority of CH_4 is converted to CO_2 with some small formation of CO. During the initial 600 seconds of the oxidation period all of the oxygen is absorbed by the sample, with a subsequent rapid return to the inlet concentration. There is limited formation of carbon on the sample during reduction as indicated by the relatively small CO_2 peak during the beginning of the oxidation period, cf. *Figure 3.1b* at 1950 s, typically corresponding to 0.5% of the total carbon supplied.

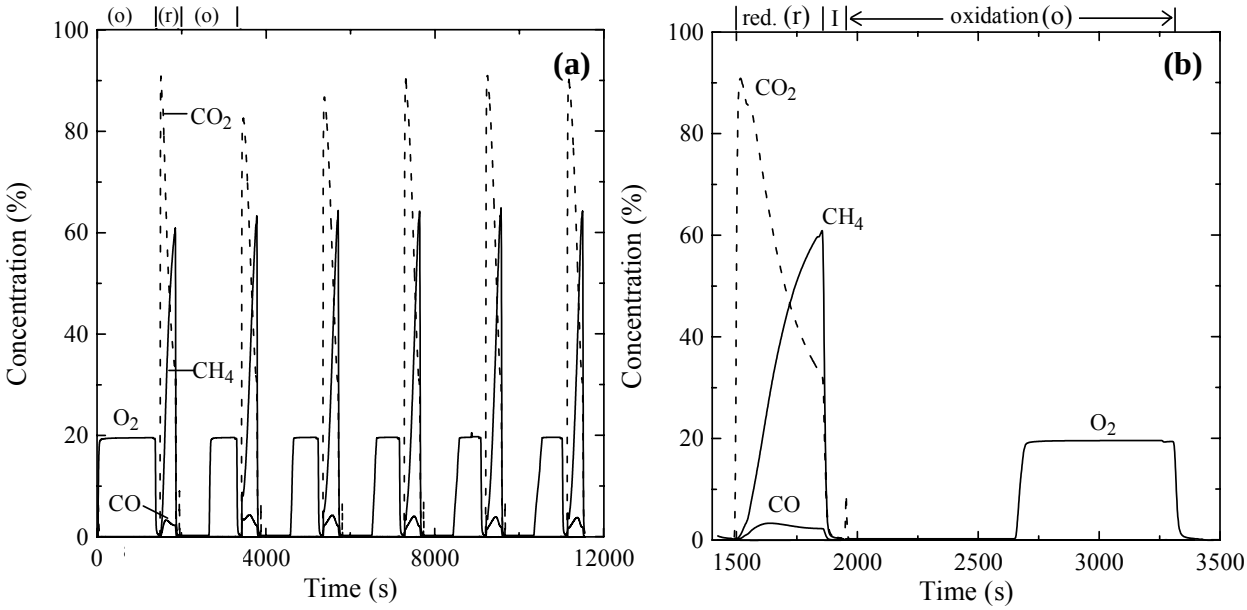

Figure 3.1 (a) The outlet concentrations of CH_4, CO_2, CO and O_2 as a function of time using natural iron ore (90 g bed material; CH_4 360 s; air 1330 s).
(b) The outlet concentration of CH_4, CO_2, CO and O_2 for the first reduction period (r) and second oxidation period (o). Period denoted by I is the time when the reactor is flushed with inert gas for 120 s.

The conversion, X, as a function of time varied between 100% (Fe_2O_3) and about 87% during each cycle, i.e. ΔX=13%, for the experiment in *Figure 3.1a and b*. Here, X is based on the

conversion from Fe_2O_3 to Fe, i.e. m_{ox} is mass of Fe_2O_3 and m_{red} is mass of Fe. From x-ray powder diffraction of reacted samples it was found that the only major phase present after oxidation was α-Fe_2O_3, which indicates that the samples were fully oxidized during the oxidizing periods.

The average rate of reduction of the iron ore, as measured over an entire reduction period, is shown as a function of the gas yield of CH_4 to CO_2 in *Figure 3.2a* and conversion range as a function of the gas yield in *Figure 3.2b*. The data points in *Figure 3.2a* represent the average rate for either the first or sixth reduction period for experiments using bed masses between 15 - 90 g and reduction periods of 180 s - 720 s. The data for the shorter time periods, 22 - 90 s, are taken from the experiments conducted with 180 s reduction periods. The rate of conversion of Fe_2O_3 varied from 1 - 8%/min with the yield of CH_4 to CO_2, (cf. *equation 2.1*), ranging between 10 and 99%.

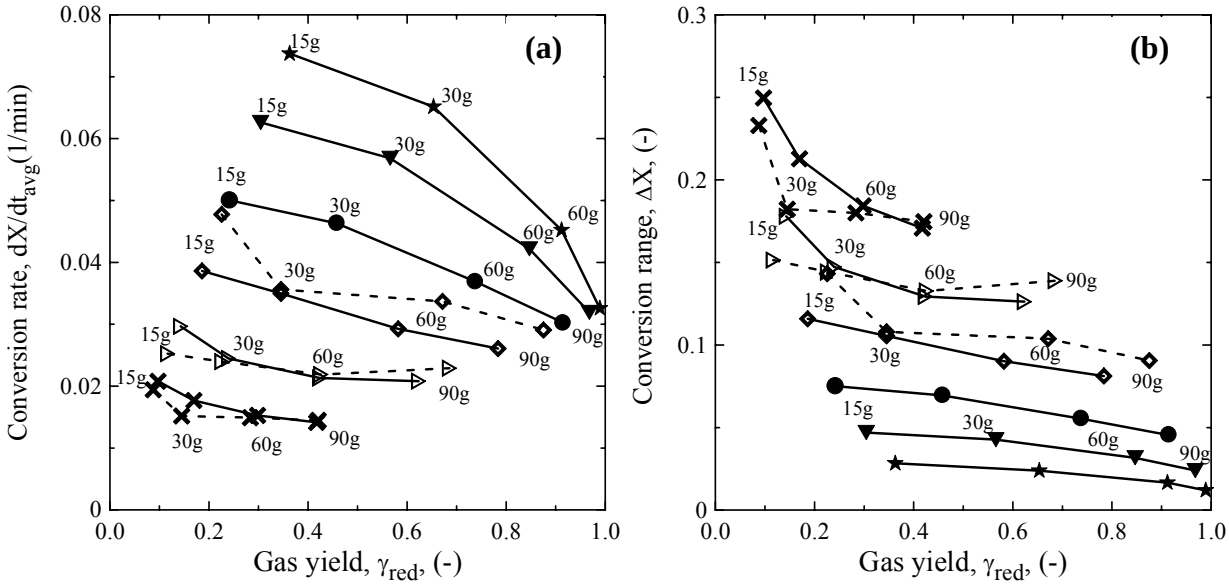

Figure 3.2 (a) The average rate of reduction, dX/dt_{avg}, for an entire reduction period as a function of the average degree of yield of CH_4 to CO_2, γ_{red}, using bed masses of 15 - 90 g and reduction periods of 180 s - 720 s. Each data point represents the average rate for either the first (solid lines) or sixth (dashed lines) reduction period. The data for the shorter time periods, 22-90 s, are derived from the initial part of the experiments conducted with 180 s reducing period. The time under reducing conditions is: 22 s (★), 45 s (▼), 90 s (●), 180 s (◆), 360 s (▷), 720 s (✖).
(b) The conversion difference, ΔX, shown as a function of the gas yield, γ_{red}, for the experiments in *Figure 3.2a*.

The rate is greatest for experiments with small beds and short reduction times. In the case of small beds, this is explained by the higher concentration of methane to which the sample is exposed, whereas a short reduction time means that the sample reacts in a small conversion interval where the rate is high. Thus, greater rates of reduction and gas utilization are achieved by

lowering the time under reducing conditions. This means that the conversion range also decreases.

In these experiments, which were suited for investigation of the reduction rate, e.g. *Figures 3.1* and *3.2*, all of the oxygen was consumed during the initial part of the oxidation. Therefore the oxidation rates obtained, 1-6%/min, were limited by the oxygen supply.

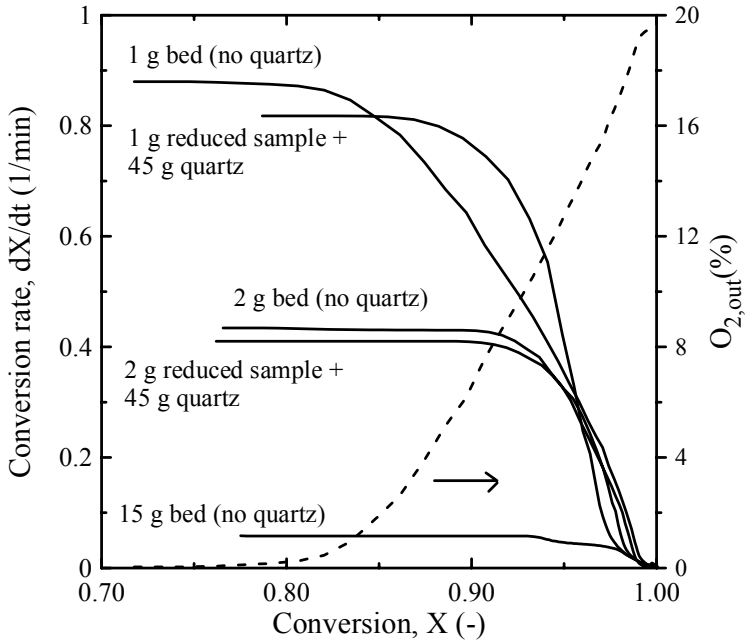

Figure 3.3 The oxidation rate of reduced iron ore as a function of the conversion (solid lines) for experiments conducted with i) 1 and 2 g beds without the addition of quartz using reactor II, ii) 1 and 2 g reduced iron oxide + 45 g quartz and iii) 15 g bed without the addition of quartz. The set-point temperature was 950°C and the air flow 900 mL/min. For the 1 g bed without quartz addition the oxygen concentration is also shown (dashed line).

In order to investigate the rate of oxidation it was necessary to perform experiments with smaller amounts of bed material. In *Figure 3.3* the rate is shown as a function of the conversion for experiments using iron ore samples of 1 and 2 g, which were oxidized using an air flow of 900 mL/min following reduction with 100% CH_4 for 6 minutes. Even with a bed size of 1 g and an air flow of 900 mL/min, the oxygen is rapidly consumed during the initial reaction period, followed by a drop in the rate as the conversion approaches unity. The initial reaction rate of about 90%/min is clearly limited by the oxygen supply

The original hematite material consisted of a rather nonporous material of low BET surface, about 3.7 m^2/g. A secondary electron image of a few of the unreacted particles is shown in *Figure 3.4a*. The particles have a rather irregular shape with a smooth texture. However, when the

particles were exposed to alternating oxidizing and reducing conditions the surface changed to a more coarse texture with the development of cracks and fissures in the particle. This can be observed in the picture shown in *Figure 3.4b*. Here, hematite particles which were exposed to 180 s of CH_4 and 665 s of air for six cycles are shown. However, even though there was crack development in the particles, the primary particles generally remained intact with some fragmentation and breakage.

From x-ray powder diffraction of the reacted material it was found that only FeO and Fe_3O_4 were formed during the reduction. Metallic iron was found only after 20 min reduction, and then only in minor amounts. Analysis of the iron oxide samples after oxidation showed that only α-Fe_2O_3 was present, which is the stable form of iron oxide at the temperatures used in this work.

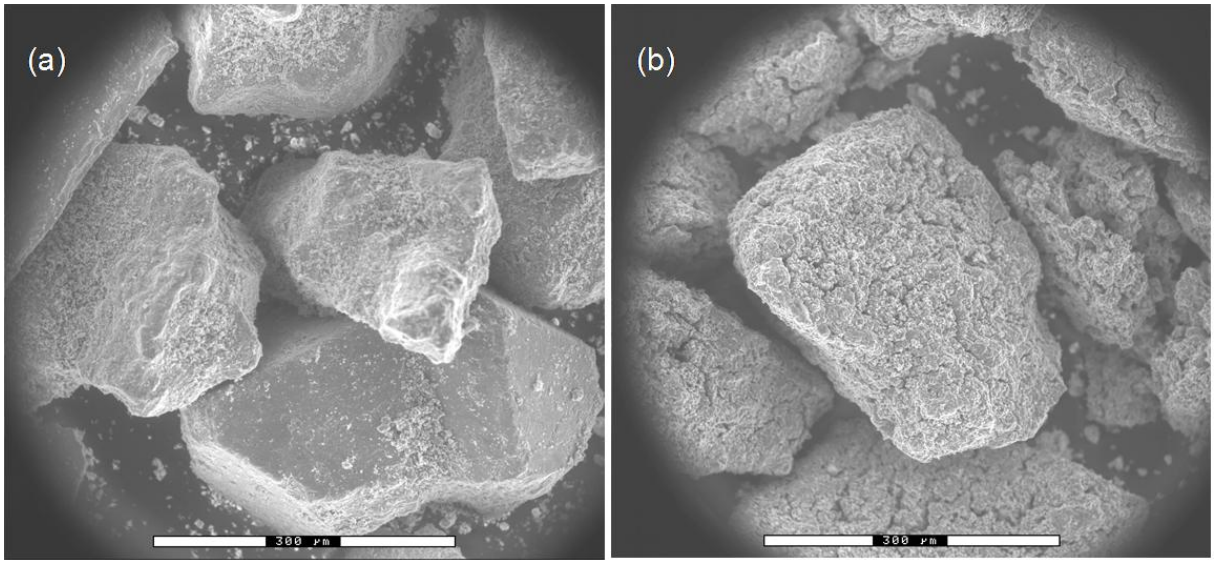

Figure 3.4 Secondary electron image of (a) unreacted hematite particles and (b) hematite particles which were exposed to six alternating cycles of 180 s CH_4 and 665 s air. The white marker indicates a length of 300 µm.

3.2 Fluidized bed reactor experiments with iron oxide based oxygen carriers (paper II)

In general, for all of the experiments where the redox reaction was investigated, the outlet concentration of CH_4, CO, CO_2 and O_2 showed qualitatively similar behavior as the experiment in *Figure 3.1a and b* with exception that the content of O_2 in the oxidation gas was 5%.

In *Figure 3.5*, the gas yields for the second reduction period are shown as function of the conversion range, ΔX. For the particles of 60% Fe_2O_3 and 40% Al_2O_3, i.e. SYN7 in *table 2.1*,

Figure 3.5a shows that high values of γ_{red}, above 90%, can be maintained for ΔX up to about 10% for the largest bed masses, while the gas yield falls with decreasing mass of bed material. The gas yields of SYN7 with a larger particle size, are somewhat lower, *Figure 3.5b*. SYN9 with the lowest content of iron oxide, 40%, showed the highest gas yields, while SYN8 with the highest content, 80%, resulted in a lower gas yield, *Figure 3.5c*. SYN10, with 60% Fe_2O_3 and 40% MgO, gave a poor gas yield.

The reduction rate, dX/dt, is shown as function of the conversion range, ΔX, and gas yields, γ_{red}, for the different oxygen carriers in *Figure 3.6*. High conversion rates are observed for SYN7 in the size range 125-180 μm, *Figure 3.6a*, as well as for the larger size fraction, *Figure 3.6b*. The reduction rate rises with decreasing amount of sample because the rates are limited by the supply of methane when γ_{red} is high. When conversion range and gas yield are considered the highest conversion rates for all samples are noted for SYN9, *Figure 3.6c*. Also shown in this figure are the inferior results for SYN8 and SYN10.

As in the previous study (paper I) the oxidation rate was very fast and an oxygen concentration of zero was measured in the outlet gases during most of the oxidation. The X-ray powder diffraction of the particles showed that the major phases present were Fe_2O_3 and Al_2O_3, except for SYN10 which contained Fe_3O_4 and MgO. After cyclic oxidation and reduction the major components of the samples were Fe_3O_4 and Al_2O_3 after the reduction periods, and Fe_2O_3 and Al_2O_3 after oxidation periods. For SYN10 however, the only phases seen were Fe_3O_4 and MgO both after reduction and oxidation.

The conversion range corresponding to complete reduction of Fe_2O_3 to Fe_3O_4 is about 11%, cf. *equation 2.2*. As shown in *Figure 3.5*, the average conversion was 10-12% in most cases. As mentioned, X-ray powder diffraction analyses of reacted samples confirm that Fe_3O_4 was the only reduced species formed. In terms of the system Fe_2O_3/Fe_3O_4, the conversion was thus nearly complete.

The peak temperature in the particle bed during the oxidizing period was limited to 1050°C by using "air" with only 5% oxygen, and no tendency of agglomeration of particles was noted. The particle integrity was studied by using a particle trap at the top of the reactor. The experiments lasted for 5-8 h, and after this period no significant amounts of particles were found in the particle trap and the visual study of particles with light microscope also indicates that no particle breakage occurs.

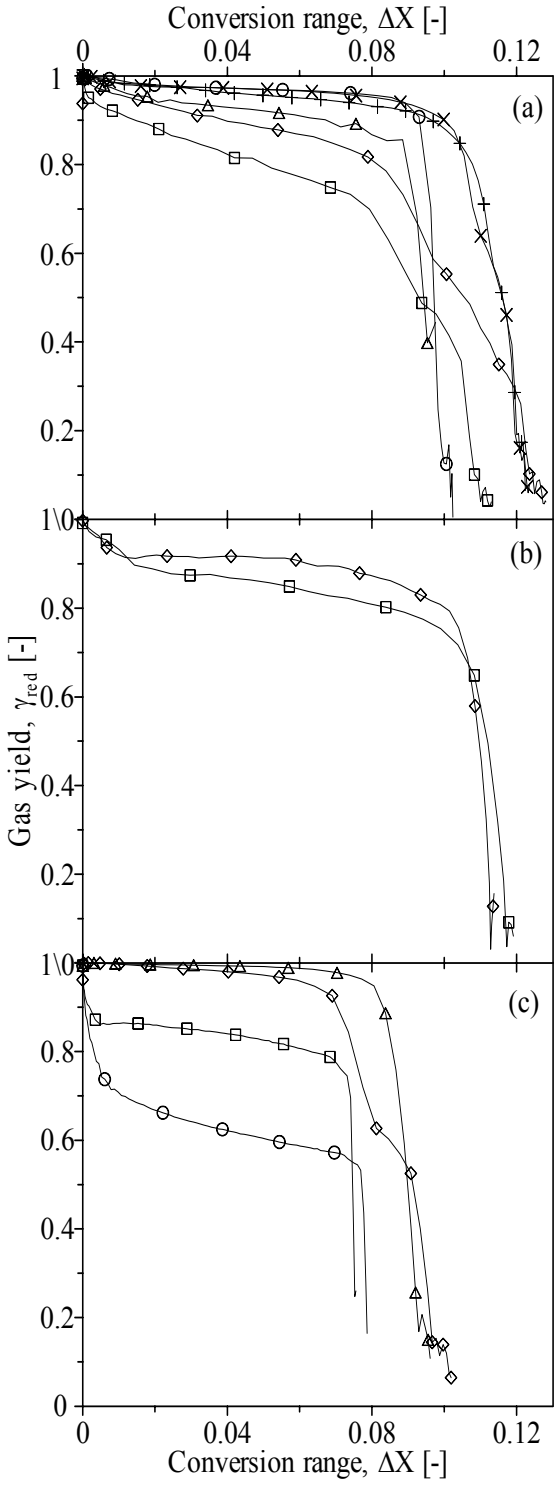

Figure 3.5 The gas yield as function of the conversion range during the second reduction cycle. (a) SYN7, *dp* = 125-180 µm: 15 g (□), 20 g (◇), 25 g (△), 32 g (○), 40 g (×), 60 g (+) (b) SYN7, *dp* = 180-250 µm: 40 g (□), 80 g (◇) (c) *dp* = 125-180 µm, SYN8: 80 g (□), SYN9: 35 g (◇), 55 g (△), SYN10: 80 g (○)

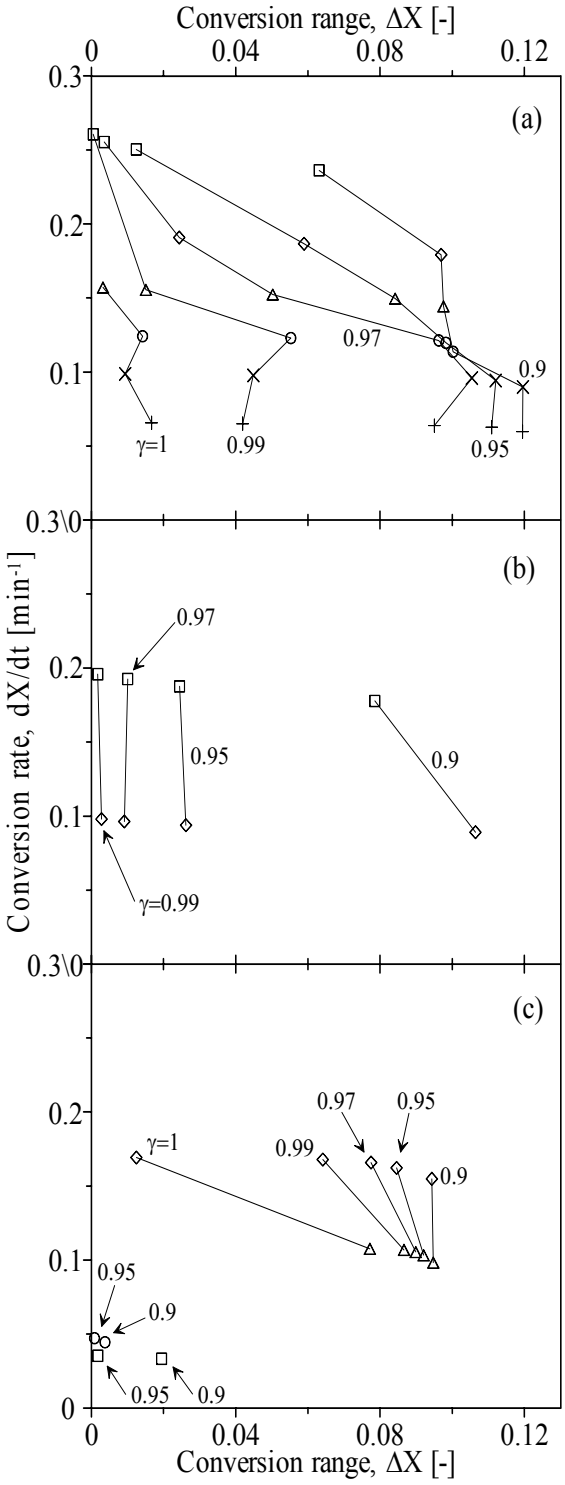

Figure 3.6 The average conversion rate as function of the conversion range for various gas yields, gred. (a) SYN7, *dp* = 125-180 µm: 15 g (□), 20 g (◇), 25 g (△), 32 g (○), 40 g (×), 60 g (+), (b) SYN7, *dp* = 180-250 µm: 40 g (□), 80 g (◇), (c) *dp* = 125-180 µm, SYN8: 80 g (□), SYN9: 35 g (◇), 55 g (△), SYN10: 80 g (○)

3.3 Fluidized bed reactor experiments with iron-, nickel-, copper- and manganese-based oxygen carriers (paper III)

In the development of suitable oxygen-carrier materials it is important to test a number of materials with varying metal oxide/support combinations and production conditions. To be able to compare larger numbers of particles, a standardized reactivity test procedure was designed. From this procedure, a single number that gives an indication of the reactivity is obtained. Thus, it is possible to show reactivity versus particle strength and agglomeration tendency. Furthermore, this reactivity number relates to the real application, and gives an indication of the amount of bed material needed in the actual process, see section 2.4.

Based on preliminary testing it was found that 10 g of sample and a methane flow of 300 mL/min was suitable for a standardized test. This amount of bed material corresponds to 57 kg/MW which is a moderate amount for an industrial application. This means that there is a complete conversion only for the most reactive materials (nickel-based), whereas the majority of the materials show a partial conversion, suitable for deriving an effective rate constant. It could be argued that a smaller amount should be used to achieve more adequate results with nickel-based materials, but this would reduce the quality of the results for the less reactive compounds. Furthermore, tests with smaller amounts of nickel-based materials without full conversion were difficult to evaluate because of side-reactions, e.g. reformation and carbon formation.

For all of the experiments where the reduction was investigated the outlet concentration of CH_4, CO, CO_2 and O_2 showed similar behavior as the experiment in *Figure 3.1 a and b* with the exception that the content of O_2 in oxidation gas was 5%.

Figure 3.7a shows the rate of mass-conversion, $d\omega/dt$, as a function of mass-conversion, ω, for all investigated oxygen carriers. Further, the gas yield, γ, is shown as a function of mass-conversion, ω, in *Figure 3.7b*. As is evident, only nickel oxide (N6AN in *Table 2.1*) is capable of converting almost all methane to carbon dioxide and water with 10 g of bed material. Below the results for each type of oxygen carrier is discussed:

Fe_2O_3 to Fe_3O_4 is the only reduction in the iron oxide system that is able to convert methane completely to carbon dioxide and water at high temperatures. Thus, for reduction to a lower iron oxide, such as FeO, it is not possible to have full gas conversion in fuel reactor. [Mattisson and Lyngfelt, 2001] A full conversion from Fe_2O_3 to Fe_3O_4 for oxygen carriers F6A, F6AS, F6K and F6KS corresponds to a $\Delta\omega$ of 0.02. The iron oxide oxygen carriers with kaolin (F6K and F6KS) showed low rates of mass-conversion and poor mass-conversion range. One possible reason for this is the formation of mullite ($Al_6Si_2O_{13}$) and amorphous quartz above 900°C which may result in a less porous material. [Couch, 1994]

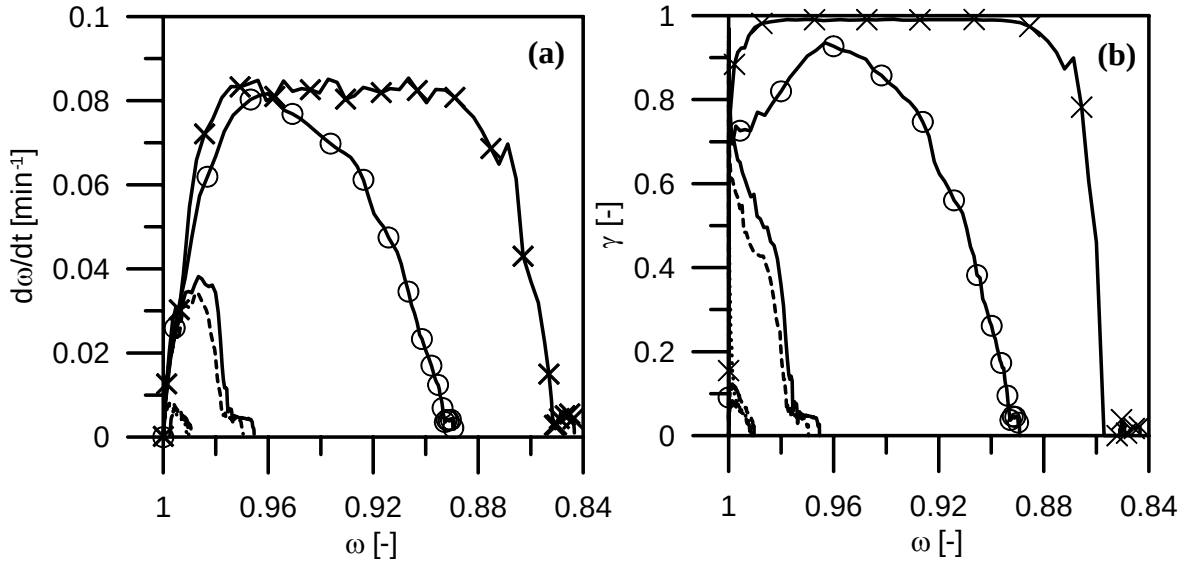

Figure 3.7 (a) The rate of mass-conversion, $d\omega/dt$, as a function of ω and (b) the gas yield, γ, as a function of ω for the second reduction period at 950°C for oxygen carriers F6A (———), F6AS (- - - - -), F6K (—·—·—), F6KS (—··—··), N6AN (—×—) and M6AM (·····), and 850°C for oxygen carrier C6AC (—○—).

The major phase in the original samples was Fe_2O_3 (and Al_2O_3 for F6A and F6AS) and in the samples taken out after a reduction period the major phase was Fe_3O_4 (and Al_2O_3 for F6A and F6AS). A slight displacement of X-ray diffraction peaks of Fe_2O_3 and Al_2O_3 was noted for F6A and F6AS, which indicates some mutual solubility of both metal ions. This has been seen in prior studies of this system [Prieto et al., 1994] A minor amount of $FeAl_2O_4$ was seen in reduced oxygen carriers with aluminum oxides. It was difficult to detect x-ray diffraction peaks indicating the presence of sintered kaolin (mullite) for F6K and F6KS, but the presence of amorphous phases was much higher compared to oxygen carriers with no kaolin in the supporting material.

For the nickel-based particles there is an almost complete conversion of CH_4 to CO_2 and H_2O (not shown). However, to be noted is the small amount of CO and H_2 which is associated with the thermodynamic limitation of NiO to convert CH_4 fully to CO_2 and H_2O at this temperature. [Mattisson and Lyngfelt, 2001]

The reduction rate for N6AN was approximately 8%/min measured for a mass-conversion range 1 to 0.90, see *Figure 3.7a*. Note that this reduction rate is the maximum possible rate, because the gas conversion is almost complete and therefore it is limited by the supply of fuel. The calculated value of $\Delta\omega$ when all available oxygen has reacted in N6AN is 0.165. Thus, the conversion was almost complete.

In *Figure 3.8*, the rate of mass-conversion during oxidation is shown. When all oxygen is consumed, the oxidation rate is 0.67%/min. This is also the initial rate for all of the oxygen carriers except copper oxide. In *Figure 3.8*, the rate of mass-conversion for N6AN is only shown

for a mass-conversion larger than 0.9. The major phases in the fully oxidized N6AN were NiO and $NiAl_2O_4$ and after reduction the major phases were Ni and $NiAl_2O_4$.

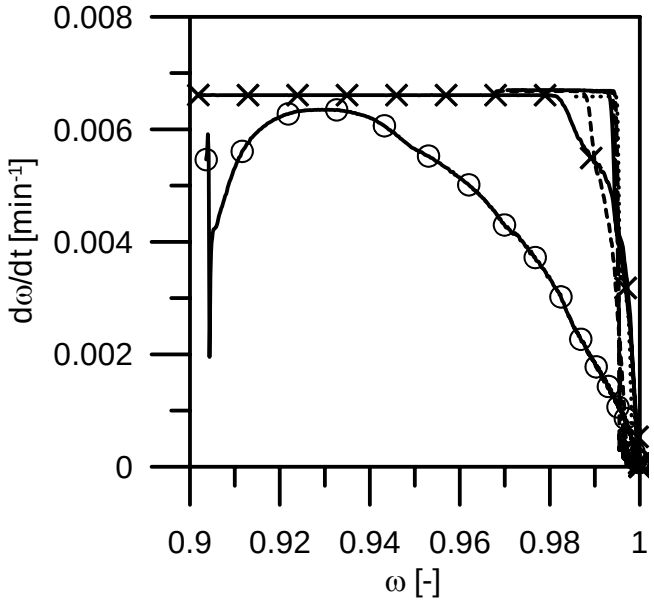

Figure 3.8 The rate of mass-conversion, $d\omega/dt$, as a function of mass-conversion, ω for the second oxidation period at 950°C for oxygen carriers F6A (———), F6AS (- - - - -), F6K (—·—·—), F6KS (—··—··), N6AN (—×—) and M6AM (·····), and 850°C for oxygen carrier C6AC (—○—).

For C6AC the reduction rate peaked at almost 8%/min, but contrary to NiO the supply of the fuel gas did not limit the reduction rate. The mass-conversion, ω, reached 0.89. The theoretical value of $\Delta\omega$ when CuO is reduced to Cu is 0.156, i.e. ω at the end of a full reduction should have been 0.844. Some oxygen was seen during the inert period following the oxidation period with an average O_2 concentration of 0.4% and even in the first half part of reduction period with an O_2 concentration as high as 1.9%. The reason is decomposition of CuO to Cu_2O which is the most stable phase at low partial pressure of oxygen and high temperature. [Mattisson and Lyngfelt, 2001] The decomposition of CuO to Cu_2O, occurs in air at temperatures above 1030°C. The existence of Cu_2O in the fresh C6AC was confirmed by XRD. Carbon dioxide and carbon monoxide were formed during the inert period (N_2) and in the beginning of oxidation period, which indicates that oxygen was taken from oxygen carrier by carbon formed during the reduction period, and the mean CO_2 and CO concentrations during inert period were 1.2% and 0.1%. Further, the maximum values reached by carbon dioxide and carbon monoxide during the beginning of the oxidation period were 3.4% and 0.08%. The total amount of C released during the inert and the oxidation period corresponds to 3.2% of the total amount of C entering the reactor during a reduction period. In contrast to the other oxygen carriers the oxidation rate was not limited by the access to oxygen, and reaches a maximum value of 0.64%/min at ω=0.93, see

Figure 3.8. The major phases in the fresh C6AC were CuO, Cu_2O, $CuAlO_2$ and $CuAl_2O_4$ and after a reduction period the major phases were Cu and Al_2O_3.

The oxygen carrier of Mn_3O_4 and $MnAl_2O_4$, i.e. M6AM in *Table 2.1*, showed low mass-reduction rate and low conversion almost comparable with F6K and F6KS even though the initial reduction rate was higher. The theoretical value of $\Delta\omega$ when Mn_3O_4 is reduced to MnO is 0.04 but reached only 0.009. One possible explanation could be low porosity, 0.02 cm^3/g. The major phases in the fully oxidized M6AM were Mn_3O_4 and $MnAl_2O_4$ and after a reduction period the major phase were MnO and $MnAl_2O_4$.

If the mass transfer resistance between bubbles and emulsion phase in the fluidized bed is negligible and assuming that the reaction is first order with respect to methane, the effective rate constant is useful to evaluate reactivity since it is not dependent of the concentration of methane in the fuel reactor. As in *Figure 3.1b*, all of the oxygen in the reactor was consumed during the first part of the oxidation period which suggests a good contact between the gas and the particles. The effective rate constants, $k_{\omega,\text{eff}}$ is shown as a function of ω in *Figure 3.9*. Since the exiting partial pressure of CH_4 is almost zero for the NiO sample (N6AN) it is not possible to calculate a meaningful rate constant from *equation 2.11*. In order to obtain at least a "minimum value" of $k_{\omega,\text{eff}}$ during full methane conversion, the outlet concentration of methane used to calculate the log-mean partial pressure, $p_{CH_4,\text{out}}$, was set to 1%.

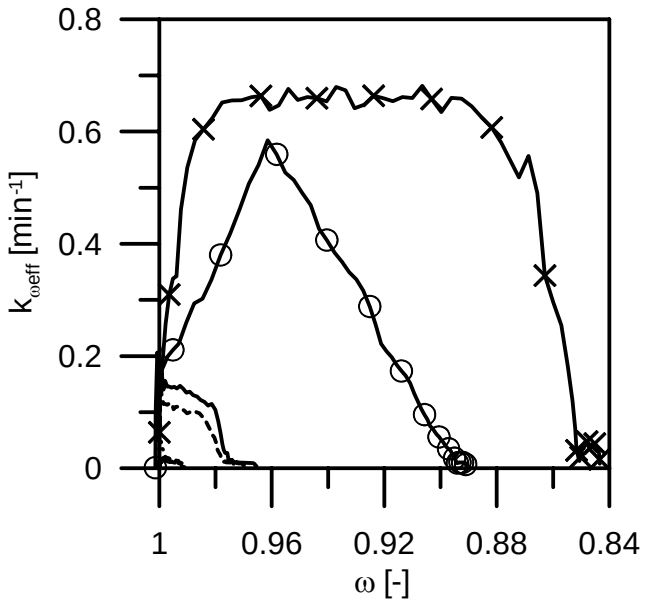

Figure 3.9 The effective mass-constant, $k_{\omega,\text{eff}}$, as a function of mass-conversion, ω for the second reduction period at 950°C for oxygen carriers F6A (———), F6AS (- - - - -), F6K (— · — · —), F6KS (— · · — · ·), N6AN (—×—) and M6AM (·····), and 850°C for oxygen carrier C6AC (—○—).

Some of physical properties of the particles are shown in *Table 3.1*. The size range of the fresh oxygen carrier particles used in the test of crushing strength was 0.180 - 0.250 mm and the values shown in *Table 3.1* were based on 20 measurements. Generally, the BET area was rather low for all samples. N6AN had the highest active area (BET) value, 2.46 m^2/g followed by M6AM, 1.25 m^2/g. F6K, F6KS and C6AC showed lowest value of active area, about 0.3 m^2/g. The mean values of crushing strength of oxygen carriers varied between 0.3 and 20.6 N and the standard deviation was between 0.3 and 9.2 N. The crushing strength of the oxygen carriers was correlated to the apparent densities with the denser samples having the highest crushing strength. N6AN showed largest pore volume, 0.30 cm^3/g, thereafter iron oxide samples with alumina, 0.10 (F6A) and 0.12 cm^3/g (F6AS). The samples of the iron oxide with kaolin, copper oxide and manganese oxide showed almost no pore volume. A small increase of pore volume was observed in samples with starch in the slurry (F6AS and F6KS). The surface of oxygen carriers was studied with electron microscope before and after six reduction and oxidation periods, see *Figure 3.10*. All the oxygen carriers, with the exception of C6AC, had small granular surfaces and N6AN showed the smallest grains. There were no particular differences in surface structure between fresh and used oxygen carriers.

Table 3.1 The physical properties of oxygen carriers.

Oxygen carrier	Density (g/mL)	BET (m^2/g)	Porosity (cm^3/g)	Crushing strength (Standard deviation) (N)	paper
F6A	3.2	0.96	0.10	5.6 (1.6)	III, IV, V
F6AS	2.8	0.84	0.12	4.7 (1.6)	III
F6K	3.5	0.28	0	20.6 (9.2)	III
F6KS	3.2	0.36	0.02	11.2 (2.7)	III
N6AN	1.9	2.46	0.30	0.3 (0.1)	III, IV
C6AC	3.4	0.31	0.02	4.3 (1.4)	III
M6AM	1.8	1.25	0.02	0.9 (0.3)	III
M4Z	2.1	-	-	0.7 (0.2)	V
N6AN1300	2.1	-	-	0.4 (0.1)	V
N6AN1400	2.4	-	-	0.7 (0.2)	V
N6AN1500	3.1	-	-	1.5 (0.2)	V
N6AN1600	3.7	-	-	2.7 (0.5)	V
Quarts sand*	-	NA	NA	9.2 (3.8)	-

* Included for comparison

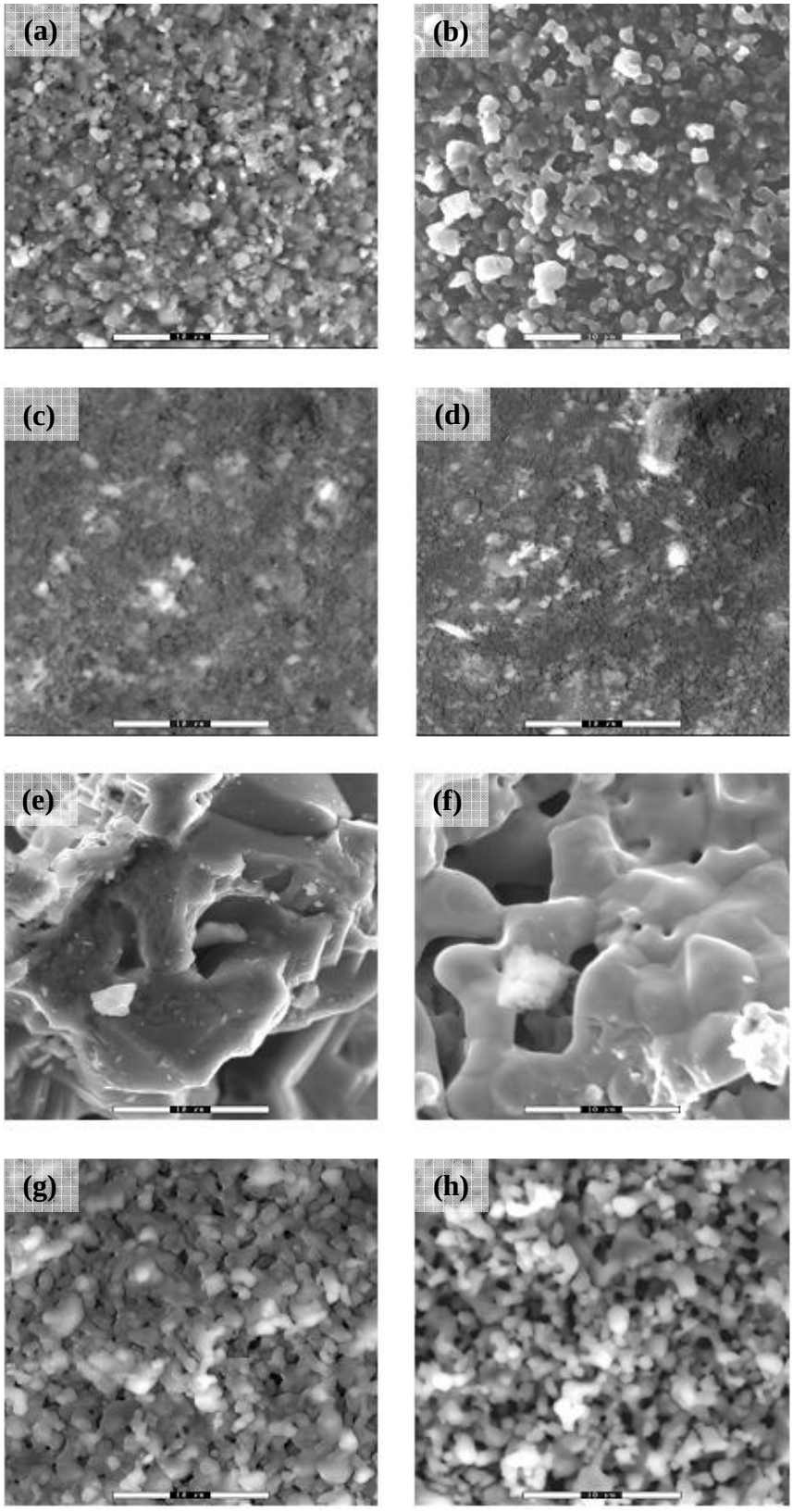

Figure 3.10 ESEM images of surface of fresh and reduced oxygen carrier particles. The magnification of the image was 3800 times. The white marker indicates a length of 10 µm. (a) fresh F6A, (b) reduced F6A, (c) fresh N6AN, (d) reduced N6AN, (e) fresh C6AC, (f) reduced C6AC, (g) fresh M6AM, (h) reduced M6AM

3.4 Carbon formation on the oxygen-carrier particles (paper IV)

In papers I-III it was found that there could be some carbon formation on Ni, Cu and Fe oxygen carriers. To get a better understanding of when carbon is formed, the carbon deposition was investigated as a function of the gas and solid conversion for Ni and Fe based oxygen carriers. The experiments were carried out in a fluidized bed quartz reactor and the time under reducing conditions was varied. In *Figure 3.11*, the outlet concentrations of CO_2, CO, CH_4, and O_2 are shown as functions of time for the oxygen carrier N6AN using pure CH_4. The lengths of the reduction period in *Figure 3.11* are (a) 80, (b) 110, and (c) 180 s.

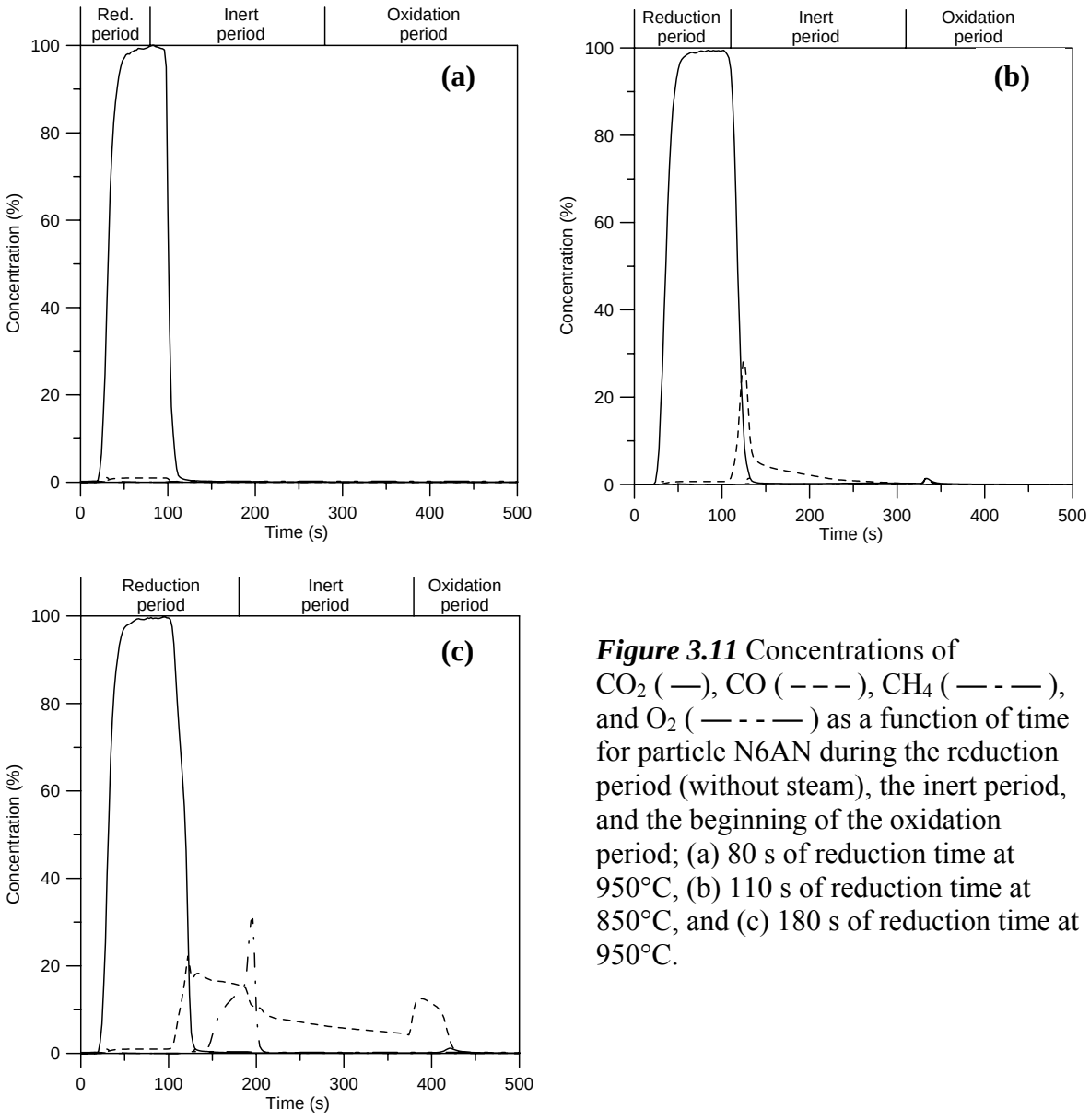

Figure 3.11 Concentrations of CO_2 (—), CO (– – –), CH_4 (— - —), and O_2 (— - - —) as a function of time for particle N6AN during the reduction period (without steam), the inert period, and the beginning of the oxidation period; (a) 80 s of reduction time at 950°C, (b) 110 s of reduction time at 850°C, and (c) 180 s of reduction time at 950°C.

In *Figure 3.11a-c*, because of the residence time of the gases between the three-way valve and the gas analyzer, the outlet gas concentration signal is delayed by 15-20 s depending on the flow rate of the gas. During the first 100 seconds of *Figure 3.11a-c*, almost all of the reacted CH_4 is converted to CO_2 and H_2O. In *Figure 3.11b and c*, as the reactions proceed, the oxygen in the particles is depleted, and the outlet concentration of CO_2 decreases, whereas the concentrations of CO and CH_4 increase. The subsequent slow decrease of the CO concentration in the inert period and peaks of CO and CO_2 in the beginning of the oxidation period indicate carbon formation during the previous reduction period. In contrast, in *Figure 3.11a*, almost no carbon was formed during the reduction period, as seen from the low CO and CO_2 concentrations throughout the inert and oxidation periods. Nevertheless, the low and decreasing CO concentration in the inert period indicates that a small amount of carbon has been formed during the reduction period.

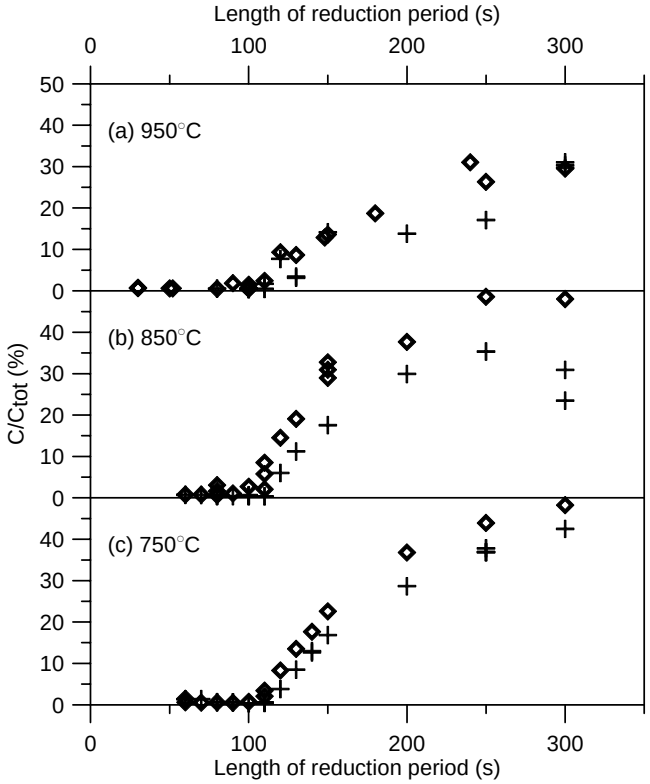

Figure 3.12 Carbon formation ratio, C/C_{tot}, as a function of length of reduction period, without steam (◇) and with 50% steam (+) for particle N6A; (a) 950°C, (b) 850°C, and (c) 750°C.

The carbon formation ratio, C/C_{tot} *(equation 2.17)*, is shown in *Figure 3.12* versus reduction time, for N6AN at 950°C, 850°C, and 750°C. The carbon formation ratios were low for N6AN at all investigated temperatures up to 100 s, see *Figures 3.12a-c*. It is clearly seen that the carbon formation ratios are lower with 50% steam present, but the difference is rather small. After 100 s the carbon formation ratios increased with the length of the reduction period. Less carbon was

produced at higher temperature. It should be mentioned that all available oxygen left in the N6AN would be consumed when the reduction period exceeds 120 s, if full conversion of the methane is assumed.

The gas yield at breakpoint is the momentary value of gas yield at the moment that the reduction period ends and the inert period starts. Due to the time delay caused by gas residence time, the gas yield at breakpoint is defined when the sum of CO_2, CO, and CH_4 is decreased by 50%, i.e. in the middle of the transient. The C/C_{tot} as a function of the gas yield at breakpoint for oxygen carrier N6AN at 950°C, 850°C, and 750°C is shown in *Figures 3.13a-c*. For all investigated temperatures, major amounts of carbon formed only for low values of gas yield at breakpoint. This indicates that major carbon formation starts only after the particles have lost so much oxygen that they are not able to convert much of the fuel.

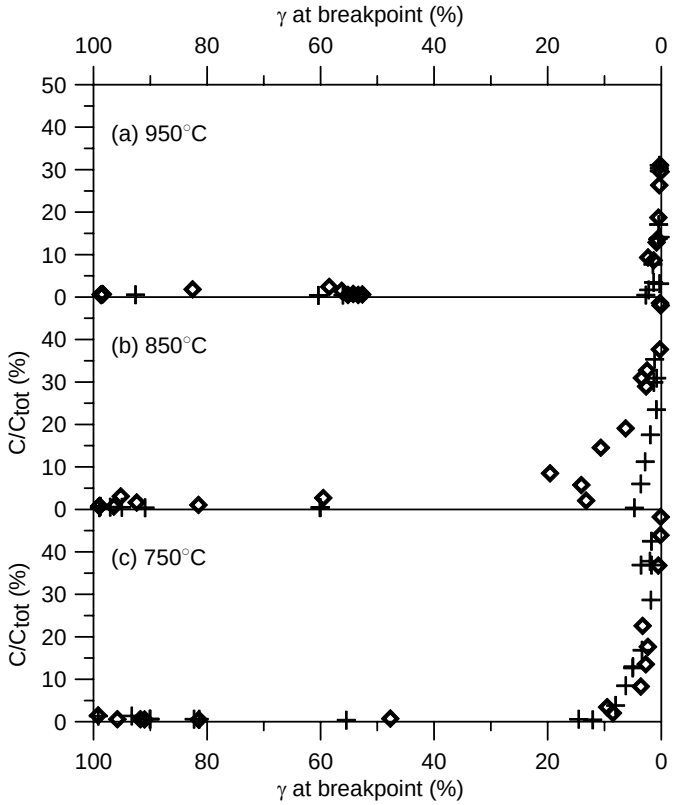

Figure 3.13 Carbon formation ratio, C/C_{tot}, as a function of the gas yield at breakpoint, γ, i.e. at the end of the reduction period without steam (◇) and with 50% steam (+); (a) N6AN, 950°C, (b) N6AN, 850°C , and (c) N6AN, 750°C.

For the iron-based oxygen-carrier, F6A, there was no carbon formation, except for a very small amount formed after 300 s of reduction period (not shown).

Paper V treats defluidization, however, additional results were also obtained for carbon formation on manganese based oxygen-carrier particle, M4Z. The results for nickel and iron

particles were similar with the tests in paper IV. The C/C_{tot} for M4Z was 2% for the short reduction period (50 s), and 1% for the long reduction period (400 s).

In paper V, it is also concluded that there is a distinct difference in the carbon oxidation behavior of Ni in comparison to Fe and Mn. Thus, it is seen that the carbon is oxidized by lattice oxygen for Ni during the inert period, *Figures 3.11b, and c*, whereas the oxidation of carbon for Mn and Fe only occurs in the oxidation period, see *Figures 3.14 c, and d* (only for Fe was shown). A similar type of behavior has also seen for Ni, Mn, and Fe supported on SiO_2. [Zafar et al. 2005]

During the study of carbon formation in paper IV, interesting observations regarding defluidization were also made. All experiments with F6A resulted in agglomeration if the reduction period lasted longer than 70 s. This was seen both in the absence and in the presence of steam. However, the particles were still fluidized, i.e., there was no agglomeration, after 20 oxidation/reduction cycles when the length of the reduction period was kept at 50 s. This was seen both with and without addition of steam. This suggests a strong influence of the extent of reduction of the particles and defluidization, which was further explored in paper V.

3.5 Defluidization (paper V)

The defluidization behavior of Ni, Mn and Fe based oxygen carriers was investigated, see *Table 1* of Paper V for a description of the particles investigated. Defluidization has been studied by measurements of the pressure drop and the pressure drop fluctuations over the particle bed and by varying the length of the reduction period.

Outlet gas concentrations of CO_2, CO, CH_4, and O_2 are shown as function of time for reduction and oxidation of oxygen carrier particles F6A in *Figure 3.14*. The upper graphs (a) and (b) in *Figure 3.14* show a short reduction period and the subsequent oxidation period, whereas the lower graphs (c) and (d) show a long reduction period and subsequent oxidation period. The length of reduction and oxidation periods in Figure 3.14 are; (a) reduction period: 40 s, (b) oxidation period: 700 s, (c) reduction period: 100 s, and (d) oxidation period: 1000 s. The length of inert periods between reduction and oxidation is 200 s. Because of the residence time between the three-way valve and the gas analyzer, the outlet gas signal is delayed 15-20 s depending on the flow rate of the gas. In general, as the length of the reduction period is increased, the length of the subsequent oxidation period is increased, since more of oxygen is removed from the particles during the reduction

In the beginning of the reduction periods in *Figure 3.14*, a large part of the CH_4 is converted to CO_2 and H_2O for iron and manganese (not shown) based oxygen carriers, and for nickel oxide

(not shown) based oxygen carriers, almost full conversion of CH_4 was achieved. As the reactions proceed, the oxygen in the particles is depleted, and the outlet concentration of CO_2 decreases, whereas the concentrations of CO and CH_4 increase.

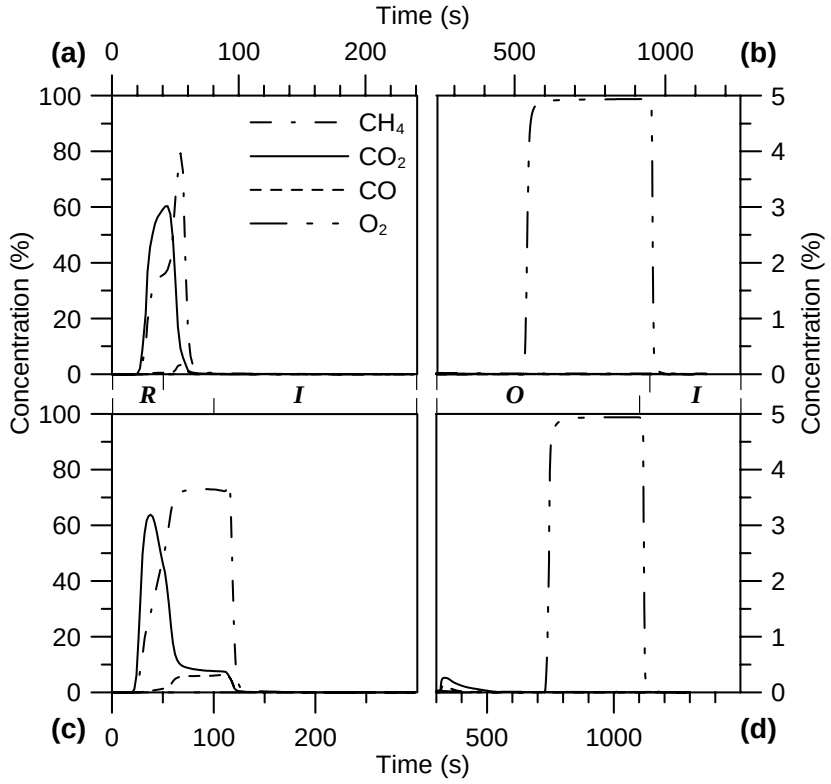

Figure 3.14 Concentrations of CO_2, CO, CH_4, and O_2 as a function of for F6A particles during a short (a-b), and long (c-d) cycle (reduction-inert-oxidation-inert). Time periods are shown in Table 4, paper V. The ticks between the upper and lower diagram show when the three way valve switches to the different gas streams: reducing period (*R*), oxidation period (*O*), and inert period (*I*).

In *Figure 3.14b and d*, the outlet concentration of oxygen was zero during a large part of the oxidation period followed by a rapid increase to the inlet concentration. This indicates that all of the O_2 going into the reactor was fully consumed and the rate of the oxidation was limited by the supply of O_2 to the oxygen-carrier particles. The lengths of the oxidation periods were chosen to ensure that full oxidation of the oxygen-carrier particles were attained.

Examples of measurements of the pressure drop over the reactor are shown in *Figure 3.15*. These pressure drop fluctuations measurements were used to indicate when the bed defluidized. The stop in fluidization is characterized by a significant drop in pressure fluctuation as well as by some decrease in the total pressure drop. The latter could be explained by channel formation in the defluidized bed. *Figure 3.15a* shows the pressure drop over the reactor during an oxidation

period, followed by inert, reduction, inert and finally an oxidation period for F6A. Here the bed is defluidized early in the last oxidation period. A typical defluidization is shown in *Figure 3.15b*, showing the magnified pressure drop when the bed is fluidized and defluidized.

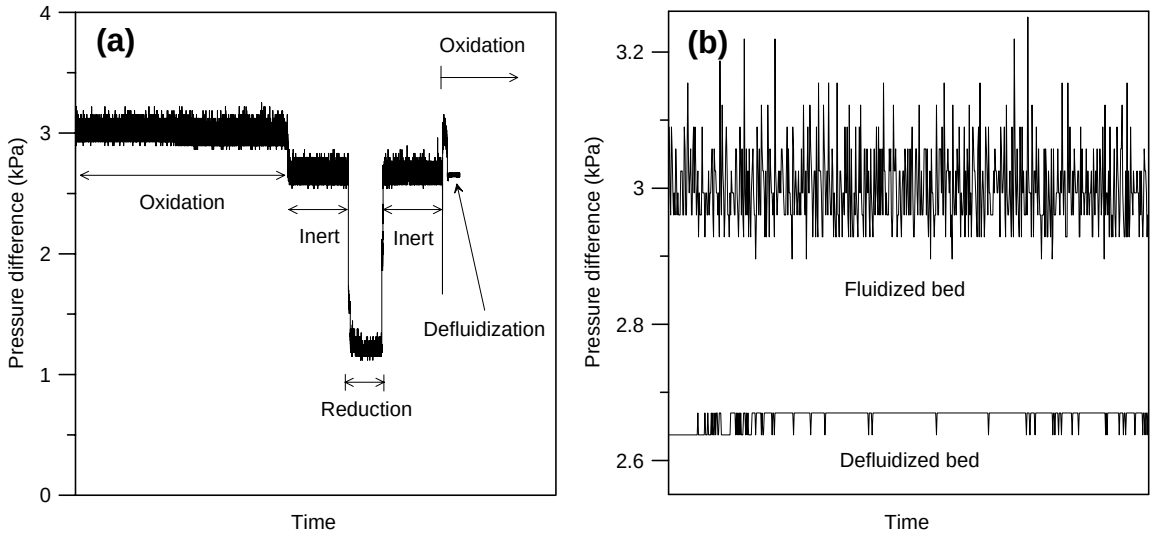

Figure 3.15 Pressure drop over the reactor: (a) oxidation period followed by inert, reduction, inert and finally an oxidation period where the bed is defluidized (case FC) and (b) enlargement of parts of oxidation periods from (a) when bed is fluidized and defluidized.

A description of the cases studied and the time under reducing conditions can be found in *Table 2* of Paper V. There was no defluidization of the iron particle bed, case FD, when the length of reduction was kept at 40 s for 40 reduction-oxidation cycles. In contrast, all the cases of defluidization of the bed with nickel oxide based particles occurred at the end of reduction period or beginning of the subsequent inert period (not shown, cases NC, ND and NE). A major difference between the defluidized beds obtained for iron and nickel oxide based particles was that the iron oxide particles formed a rather hard agglomeration while the nickel oxide particles were still loosely packed. In the latter case the bed could be even poured out of the reactor after the test.

The mass conversions after the reduction, ω, and the length of the reduction period, t_{red}, are shown versus cycle number in *Figures 3.16a and b*, for particle F6A (cases FA-FE). In cases FA-FC, the length of the reduction period was gradually increased until the bed was defluidized. In almost all cycles the change in mass conversion, $\Delta\omega$, was 2% or more, corresponding to ω values below 0.98, see *Figure 16a*. All cases of fluidization occured at a high $\Delta\omega$, the lowest being 3% in case FA.

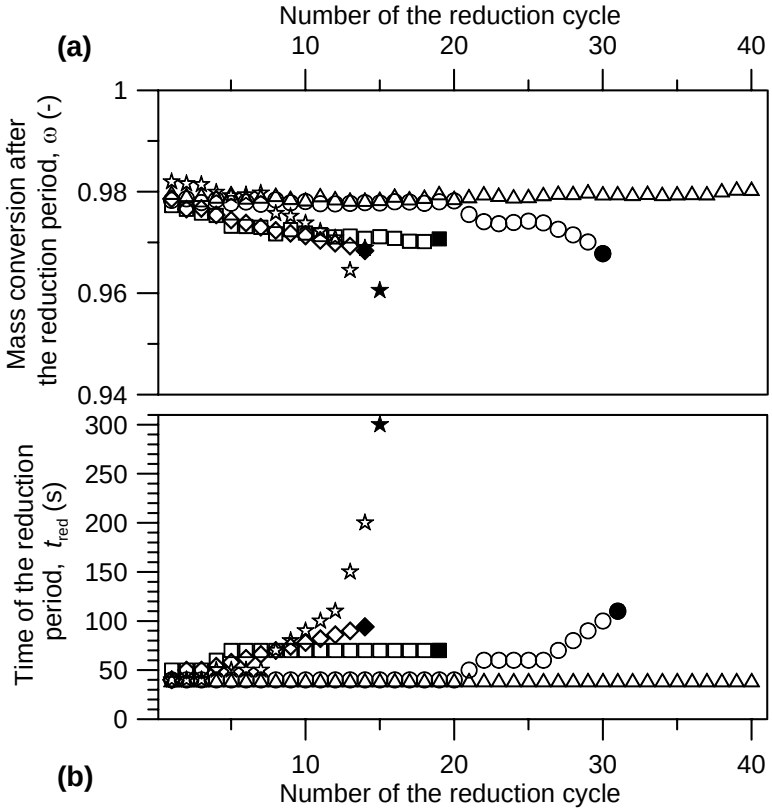

Figure 3.16 The mass conversion after the reduction period, ω, (a), and the time of the reduction period, t_{red}, (b), as a function of number of the reduction cycle for: (◇) Case FA, (□) Case FB, (○) Case FC, (△) Case FD, and (☆) Case FE. Filled symbols denote defluidized bed.

The change in mass conversion is a function of the length of the reduction period, as shown in *Figure 3.17*. The results show high reproducibility, with the exception of the tests made in reactor V, case FE. Especially the last cycle before defluidization occurs, which is the one at 200 s, deviates markedly in case FE. It can be speculated that this deviation could be caused by partial defluidization.

According to the definition of conversion, X (see *equation 2.2*), for the Fe_2O_3-Fe_3O_4 system, the conversion reaches 0%, i.e. the reduction is complete, when the mass conversion reaches 98%. However, most of the mass conversion values exceed 2% in *Figure 3.17*, and this is explained by the further reduction of Fe_3O_4 (magnetite) to FeO (wustite). This is possible only because of the low conversion of the fuel since the further reduction to FeO cannot, thermodynamically, oxidize the fuel fully to CO_2 and H_2O. [Mattisson and Lyngfelt, 2001] This also means that in a real application of a chemical-looping combustor, where more or less complete oxidation of the fuel to CO_2 and H_2O takes place, this further reduction to FeO would not be expected.

As can be seen in *Figure 3.17*, a conversion of 0.98 is obtained after approximately 40 s reduction. A reduction period of 40 s is seen in *Figure 3.14a* and just at the end of the reduction period there is a sharp increase in methane. As can be seen in *Figure 3.14c* where the reduction cycle is longer, the gas concentrations stabilize at a rather low level of conversion after an initial period of approximately 40 s. There is good reason to attribute this change in behavior after 40 s, to a shift from reduction to magnetite to reduction to wustite.

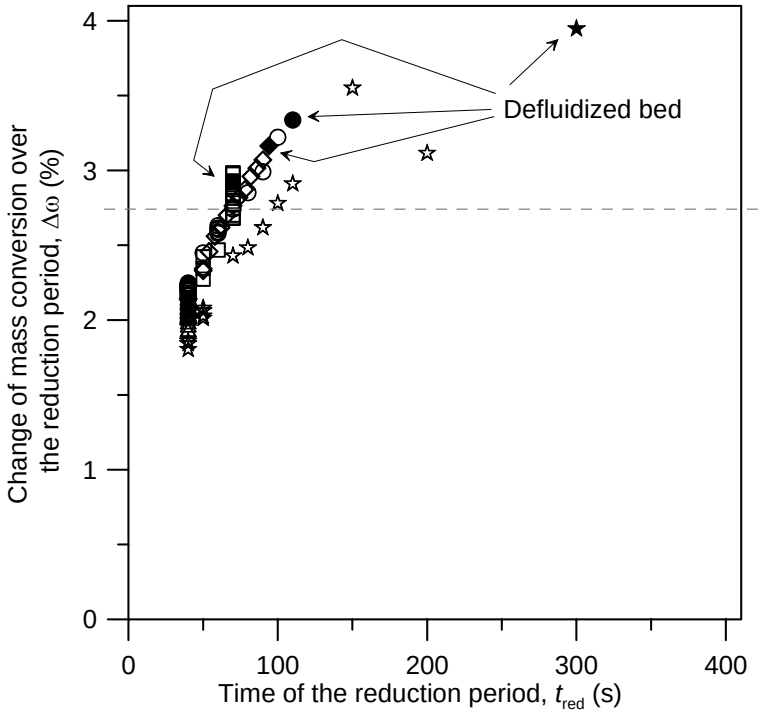

Figure 3.17 The change of the mass conversion over the reduction period, $\Delta\omega$ as a function of the time of the reduction period: (◇) Case FA, (□) Case FB, (○) Case FC, (△) Case FD, and (☆) Case FE. Filled symbols denote defluidized bed.

It is evident that all cases of defluidization has occurred at high changes in mass conversion, approximately 3% or higher, when significant amounts of FeO have formed. The formation of FeO was also confirmed by X-ray powder diffraction.

There was no defluidization of the bed of nickel oxide particles, N6AN1300 and 1400 (cases NA-NB), when the length of the reduction period was gradually increased up to 400 s. For particles sintered at the higher temperature of 1500°C, N6AN1500, the bed fluidized for most tests. However in case NC the bed was defluidized after the eighth reduction cycle after 100 s of reduction. In case NF, the length of reduction period was gradually increased up to 400 s without defluidization. Cases NG-NH were the first and second part of a two day test. The first day's test, NG, was ended just 150 s after beginning of the 25th oxidation period by stopping the inlet flow,

after which the oven was shut off. The subsequent day, NH, the particle was heated to reaction temperature, 950°C, in inert gas, and the test was continued by resuming the 25th oxidation period. The length of the reduction period was gradually increased to 400 s and no defluidization of the bed was noticed. Thus, the particles seem to generally fluidize well. Particles N6AN1600 was tested in the two cases ND-NE, where case ND was carried out with reactor type IV, and case NE was carried out with reactor type V. Both tests ended with defluidized beds during the first reduction period, and the length of these reduction periods was short, 50 s and 40 s.

The change of mass conversion rises rapidly with increased length of reduction period up to 100 s. (not shown) It is also clearly seen that the nickel oxide particles sintered at 1300 and 1400°C, i.e. case NA and NB, are the most reactive, whereas the harder, denser particles sintered at 1600°C, i.e. case ND and NE, are the least reactive.

In all reacted samples with nickel oxide particles, nickel and nickel aluminate were found in the particle with x-ray diffraction. The experiments were interrupted during the inert period after a reduction period, independent on whether the bed was defluidized or not. In cases ND and NE, nickel oxide was also found.

There was no defluidization of the bed for manganese particles, M4Z. Mn_3O_4 and zirconium oxide on fresh, and Mn_3O_4, MnO, and zirconium oxide on reacted particles were found with x-ray diffraction.

3.6 Crushing strength (paper V)

The density and crushing strength, i.e. the force needed to crush a particle, of the oxygen-carrier particles are presented in *Table 3.1*. The physical strength and the density of the nickel particles were increased as the sintering temperature was increased.

Chapter 4

Discussion

4.1 Fixed bed reactor experiments with iron ore (paper I)

Up until the study using natural iron ore as an oxygen carrier, experiments with oxygen carriers had only been conducted with synthetic oxygen carriers, often using relatively expensive materials, such as nickel oxide with yttria stabilized zirconia. Further, most of the experimental reaction data obtained in the literature up to this point was obtained under conditions of low reactant gas yield, i.e. differential conditions. Thus the aim was to obtain reactivity data of a cheap natural material under conditions of high gas yield of reactant gas to carbon dioxide. Iron ore was chosen for investigation due to the low cost and high availability.

A method to investigate the reactivity of oxygen carriers which provided data for design of a CLC system was established. This involves the determination of reaction rates as a function of the conversion range of solids as well as the gas yield of the reactant methane to carbon dioxide. In other words, the conversion of the fuel was studied versus the amount of bed material in the reactor. Thus, it was possible to have a direct estimation of the amount of bed material that could be needed in a real fuel reactor. The conversion rate was 3-4%/min at a gas conversion of 95%, see *Figure 3.2a*, which corresponds approximately to a fuel reactor inventory of 500 kg/MW_{th}, cf. Lyngfelt et al. (2001). Even though the rate is low, it was concluded that such an inventory could be feasible.

4.2 Fluidized bed reactor experiments with iron oxide based oxygen carriers (paper II)

In subsequent tests the reactor setup was improved by fluidizing the bed. As in paper I, reactivity data was determined as a function of the conversion range of solids as well as the gas yield of the reactant methane to carbon dioxide. However, in order to improve the iron oxide

reactivity under reducing conditions, synthetic iron oxide particles with various amounts of Al_2O_3 and MgO were manufactured. At high gas yields, the reactivity of the iron-alumina particles was higher in comparison to iron ore, with a reactivity of 6-15%/min at a 100% gas yield for the most reactive oxygen carrier, composed of 60% Fe_2O_3, see *Figure 3.6a*. Thus, the increased reactivity would mean that less bed material would be needed of this oxygen carrier in the fuel reactor compared to iron ore.

4.3 Fluidized bed reactor experiments with iron-, nickel-, copper- and manganese-based oxygen carriers (paper III)

To be able to test and compare larger number of particles a procedure for testing and evaluation was developed. This involved a crushing strength test and a standardized reactivity test from which a rate index was determined. The rate index facilitates the comparison of the reactivities of oxygen carriers. The rate index is shown versus crushing strength in *Figure 4.1*, for some particles based on the active oxides of nickel, copper, iron and manganese.

A detailed assessment of the solids inventory needed would require a comprehensive study of the particles with respect to reaction kinetics, as well as a model of the fluidized bed used. However, using some simplifying assumptions the rate index can be used to achieve a first rough estimation of the amount of solids needed in the fuel reactor. A rate index of 1 would then correspond to a bed mass of approximately 500 kg/MW thermal power (see discussions below for details). Furthermore, the rate index is inversely proportional to the estimated need of bed material in the reactor. Clearly a much lower amount of bed material will be needed in the fuel reactor when using nickel and copper based carriers, cf. *Figure 4.1*.

The rate index was calculated using equations (*2.11*), (*2.12*), and (*2.13*), where $(\mathrm{d}\omega/\mathrm{d}t)_{\mathrm{norm}}$ was calculated by the average effective rate constant in an interval of $\Delta\omega = 0.01$ for N6AN, C6AC, F6A and F6AS where the rate constant was highest. For M6AM, F6K F6KS the conversion was so poor that a smaller interval, $\Delta\omega = 0.005$, had to be used. The value of reference partial pressure of methane, p_{ref}, was chosen to 0.15 bar, which in theory corresponds to a methane conversion of 99.9%. The calculations above were made under the assumptions that the mass transfer resistance between bubbles and emulsion phase in the fluidized bed is negligible and that the reaction is first order with respect to methane. It should be noted that these assumptions may not always be true. For instance, García-Labiano et al. found that the reaction order with CuO is considerably less than 1. [García-Labiano et al., 2004] Nevertheless, the use of an effective rate constant gives a good estimate of the reactivity and can be used for a preliminary assessment of the needed particle inventory.

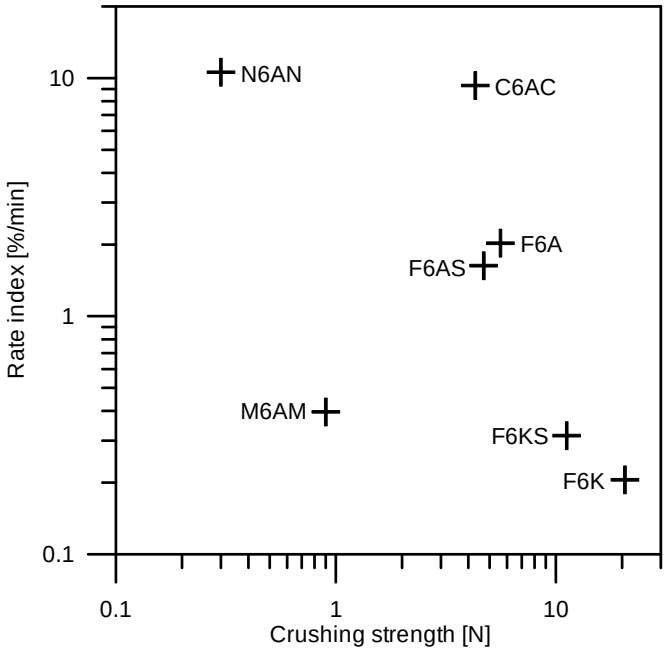

Figure 4.1 The rate index as a function of crushing strength of oxygen carriers

The low rate indexes clearly show that the particles F6K, F6KS and M6AM are not feasible as oxygen carriers. Judging from reactivity only, N6AN and C6AC seem to be excellent oxygen carriers, giving low bed masses in the reactors which reduces investment cost and need of fan power. However, C6AC agglomerated and may not be suitable as oxygen carrier. N6AN is very soft, and for use under fluidized conditions harder particles may be needed.

The rate index for N6AN is underestimated since the reaction rate was limited by the supply of gas. This is a drawback of this standardized test procedure, that the reactivity of the most reactive materials will be underestimated. However, for a first comparison, this is of minor importance.

Although F6A and F6AS require larger bed masses they may still be a good choice as oxygen carriers due to lower cost and low toxicity. The increased need of fan power due to an increased bed mass is less important in the fuel reactor since the fuel gas flow is small.

In addition to providing the necessary amount of oxygen to the fuel reactor for oxidizing the fuel completely, the hot particles must have enough sensible heat to maintain a high temperature in the fuel reactor. Because of the reactions taking place and the addition of fuel gas of lower temperature, the fuel reactor will attain a temperature different from the particles coming in, which have a temperature close to that of the air reactor. The temperature difference is a function of the oxygen carrier recirculation rate. It is important to maintain sufficient reaction temperature in the fuel reactor. In order to avoid a large temperature drop in the fuel reactor, a sufficient flow

of circulating oxygen carrier is needed, corresponding to lower $\Delta\omega$ values. This temperature difference, as well as the corresponding oxygen carrier recirculation flows, is presented in *Table 4.1* as function of $\Delta\omega$.

Table 4.1 The temperature difference in the fuel reactor for different reduction rates.

	Temperature difference in fuel reactor (°C)					
$\Delta\omega$ (-) / $\dot{m}_{sol}$ (kg/s, MW)	0.005 / 16	0.01 / 8	0.02 / 4	0.05 / 1.6	0.08 / 1	0.1 / 0.8
F6A/ F6AS	-16	-32	-63	-	-	-
F6K/ F6KS	-18	-	-	-	-	-
N6AN	-15	-30	-60	-149	-238	-298
C6AC[a]	16	31	63	157	-	-
M6AM	-12	-	-	-	-	-

[a] Calculated at 850°C.

The temperature differences in *Table 4.1* are calculated by assuming that the fuel coming in to the fuel reactor is methane at 400°C, that the fuel reactor is adiabatic, that conversion of methane to carbon dioxide and water is complete and that the temperature of the oxygen carrier particles coming from the air reactor is 950°C.

Except for copper oxide the reaction between fuel and that the oxygen carriers in the fuel reactor (*reaction 1.1*) is endothermic and the temperature in the fuel reactor will decrease, see *Table 4.1*. Note that the temperature is increased in the fuel reactor, up to 150°C, by using C6AC as oxygen carrier. This means that for copper the fuel reactor does not need to be adiabatic and that smaller recirculation flows would be possible. For the oxides of iron, manganese and nickel, the oxygen carrier circulating flow needed could be between 4 and 8 kg/s, MW_{th}, based on heat balance as well as the conversion obtained, cf. *Table 4.1*.

4.4 Carbon formation on the oxygen-carrier particles (paper IV and V)

Most studies concerning carbon deposition on oxygen-carrier were made using TGA and high concentration of reducing gas. In this study the carbon formation was investigated as function of the conversion of the fuel in order to assess if it could be a problem in a real process where high conversion of fuel is needed. From the outlet gas concentrations of carbon dioxide and carbon monoxide during the inert and oxidation period, the carbon formation on oxygen-carrier particles during the reduction period was obtained. With this approach the carbon formed also during high methane conversion may be detected.

Because there was no other source of oxygen during the inert period following the reduction period, the carbon monoxide formed during this period must be a result of oxidation of carbon formed on the particles by oxygen from the oxygen-carrier, cf. *Figures. 3.11b and c.*

For the oxygen-carrier based on nickel oxide, N6AN, the carbon formation was more dependent on the length of the reduction period, i.e. mass-conversion of the oxygen carrier, than on steam input and temperature. The amount of carbon deposition increased rapidly after 80% of the available oxygen was consumed. This rapid increase was clearly correlated to low conversion of the fuel, see *Figures 3.13a-c.*

Only a small amount of carbon was formed during the period when fuel conversion was high, mostly below 1% (C/C_{tot}) with a highest value of 1.8%. This suggests that carbon is a possible reaction intermediate and that methane conversion proceeds via carbon oxidation on the surface of the oxygen carrier.

Considering carbon formation as well as conversion of fuel, the available interval of mass-conversion, $\Delta\omega$, could be up to 10% for the N6A. The oxygen-carrier circulation mass-flow is related to the interval of mass-conversion, $\Delta\omega$, i.e. less solids need to circulate for a large $\Delta\omega$, *(equation 2.16)*. However, due to the endothermic reaction in the fuel reactor, heat must be transferred by oxygen-carrier particles from the air reactor where heat is released. Thus, the temperature difference between the air and the fuel reactor depends on the solids circulation mass-flow. For example, a $\Delta\omega$ of 10% will give approximately 300°C difference and a $\Delta\omega$ of 2% will give 60°C, see *Table 4.1*. In order to have a high enough temperature in the fuel reactor the temperature difference should be low and consequently $\Delta\omega$ must be low, i.e. a few percent. This can be compared to the high $\Delta\omega$ needed before the particles loose reactivity and carbon starts to form which is well above 10%. Thus, substantial carbon formation seems unlikely in a real application where $\Delta\omega$ has to be kept low because of the heat balance. However, the results for N6A does not necessarily apply to all nickel-based particles and more particles should be studied before any general conclusions can be made.

That carbon formation does not have to be a problem is also supported by results from a 10 kW chemical-looping combustor; Lyngfelt and Thunman (2005) reported that there was no detectable carbon dioxide in the outlet gas from the air reactor, using an oxygen-carrier based on nickel oxide.

The amounts of carbon formed on the manganese particle, M4Z, was generally low, typically 1-3.5% of the introduced amounts of carbon (CH_4) during the reduction period.

4.5 Defluidization (paper V)

The main differences between particles F6A and N6AN series were the point of defluidization and the condition of the defluidized bed. The iron oxide particle bed typically defluidized during the beginning of the oxidation, while the nickel oxide particle bed typically defluidized during the reduction period or the subsequent inert period. All the defluidized beds of iron oxide particles had agglomerated and force was needed to remove particles out from the reactor, whereas all the defluidized beds of nickel oxide particles were still loosely packed, and no force was needed to be empty the reactor. It was sufficient to turn it upside down.

For the iron oxide based oxygen-carrier, F6A, the defluidization of the bed occurred only when the change in mass conversion, $\Delta\omega$, was as high as 3% or more (case FA, FB, FC, and FE). Theoretically, the reduction of magnetite to wustite starts when $\Delta\omega$ is 2%. However, looking at an individual oxygen carrier particle, more formation of wustite at the outer shell compared to the inner part of the particle is possible. The maximum mass conversion, $\Delta\omega$, would be 6%, for full reduction of Fe_2O_3 all the way to FeO. This means that at the $\Delta\omega$ value of 3%, about one fourth of the Fe_3O_4 should be converted to wustite.

The case FD shows that there was no defluidization of the bed for forty reduction-oxidation cycles, when the change of mass conversion was kept around 2%, see *Figures 3.16a* and *3.17*. The case FE in *Figure 3.17* shows that the defluidization takes place later with reactor V, than in the other cases with reactor IV, which may be explained by different fluidizing conditions in reactor types IV and V. The reactor type V has a different shape and the velocity of the inlet gas is about four times higher than for reactor IV.

As previously noted, formation of wustite is not expected in a real application of chemical-looping combustion. Therefore laboratory experiments with iron oxide performed with long reduction times, may give an exaggerated impression of the risks of agglomeration.

The results of the present study, in combination with the results from operation of chemical-looping combustors [Lyngfelt and Thunman, 2005], show that development of iron-based oxygen-carriers that do not agglomerate has been accomplished. It is not possible to draw general conclusions on the risk of agglomeration for iron-based oxygen-carriers, but the results suggest that previous observations of agglomerations in laboratory may have been caused by the experimental conditions. Thus, assessment of agglomeration tendencies for iron oxides need careful consideration of the experimental conditions, i.e. the length of the reducing period and the degree of conversion attained.

There was no defluidization of the bed for nickel oxide based particles sintered at 1300 and 1400°C (N6AN1300 and 1400). However, the bed was defluidized during the first reduction period for particles sintered at 1600°C (N6AN1600) in both cases, i.e. ND and NE. The case NE was carried out with reactor type V. The bed of N6AN1500 particles defluidized in case NC, but the defluidization did not occur in the other tests, cases NF-H. In contrast to the tests with iron oxides no influence of the length of the reducing period could be seen. Mattisson et al. investigated NiO particles with various binder materials like $NiAl_2O_3$, TiO_2, and ZrO_2, and reported no tendency of agglomeration during reaction except for NiO/TiO_2. [Mattisson et al., 2005]

No difficulties with agglomeration during operation of particles based on nickel oxide in chemical-looping combustors have been reported. [Lyngfelt and Thunman, 2005, Ryu et al., 2004, and Johansson, 2005]

It is clear from both present tests and results from chemical-looping combustors that nickel-based particles without agglomeration difficulties can be achieved. However, no general conclusion can be made for nickel-based oxygen carriers, and it is evident that for some nickel-based particles tested there could be a risk of agglomeration.

Chapter 5

Conclusions

In this work oxygen-carrier materials for chemical-looping combustion have been studied from various aspects. For the application of CLC the work includes the first investigation of natural iron ore and freeze-granulated particles, and a number of particles based on oxides of Cu, Ni, Fe and Mn have been investigated. The work also involves the development of experimental procedures to assess the feasibility of using these materials for a real application, including tests of reactivity for estimations of the amounts of material needed, particle strength, tendencies for agglomeration and tendencies for carbon formation. Among the conclusions are:

- A method of evaluating the reactivity of oxygen carriers in fixed and fluidized beds was developed. The amount of bed material and the time under reducing conditions were varied and the rate of reduction was determined as a function of the conversion range of the oxygen carrier and the degree of methane yield to carbon dioxide. Thus it was possible to estimate the amount of material needed to convert the fuel.

- The reactivity of natural iron ore was determined in the fixed bed reactor. The reduction rates were between 1-8%min with carbon dioxide yields of 10-99% and conversion ranges between 2 and 25%. The rates obtained under a high gas yield should be sufficient to be used in a chemical-looping combustor using interconnected fluidized beds.

- Synthetic particles of iron oxide together with Al_2O_3 and MgO were prepared. Reactivity tests in the fluidized bed showed that the reduction rate at high gas yields of the methane to carbon dioxide surpassed those obtained with the natural iron ore for particles composed of 60% Fe_2O_3 and 40% Al_2O_3.

- A standardized test and evaluation procedure for oxygen-carrier particles for chemical-looping combustion was developed. The rate index obtained from a single reactivity experiment can be used to easily compare the reactivity of different oxygen carriers and also to estimate the needed solids inventory in the fuel reactor. Together with measurements of

crushing strength and observations of tendencies for agglomeration, the rate index can be used to rank the suitability of the materials.

- Seven different oxygen carriers based on iron, nickel, copper and manganese oxide were produced and tested using the simplified testing procedure. Oxygen carriers based on nickel and copper oxide with alumina as the inert showed the best reactivity. As the copper oxide particles showed signs of agglomeration, nickel oxide with alumina may be the better choice for a real process. The crushing strength of nickel-based particles sintered at 1300ºC was relatively low, but it was possible to increase the strength of these particles by raising the sintering temperature.

- There was some tendency for carbon formation on Ni-based oxygen carriers. A minor amount of carbon was formed during the most of the reduction. However, when more than 80% of the oxygen available was consumed significant carbon formation started. The formation of carbon was also clearly correlated to low conversion of the fuel. For the real application of CLC process, the carbon formation should not be a problem, because the process would be run under conditions of high conversions of the fuel.

- There was no, or very little carbon, formed on oxygen carriers of Fe_2O_3 and Al_2O_3, even when the conversion of the fuel was very low.

- The tendency for defluidization of $NiO/NiAl_2O_4$ was dependent on the sintering temperature. No defluidization was seen for the particles sintered at 1300°C and 1400°C. The particles sintered at 1500°C defluidized once, but the defluidization did not occur in the other tests. The particles sintered at 1600°C defluidized after a short reduction period. Despite defluidization the particle beds did not agglomerate.

- For the oxygen carrier of Fe_2O_3/Al_2O_3 there was no defluidization of the bed when the content of available oxygen in the particle was high. The defluidization always occurred during the oxidation period after long reduction periods, in which significant reduction of the magnetite to wustite took place. This is an important observation, because reduction to wustite is not expected in chemical-looping combustion with high fuel conversion.

- The oxygen carriers based on manganese oxide with aluminum oxide had poor reactivity. However, the particle based on manganese oxide and magnesia stabilized zirconium oxide appears to have good reactivity and showed no tendency to agglomerate. The amounts of carbon formed on the particle was generally low, typically 1-3.5% of the introduced amounts of carbon (CH_4) during the reduction period.

Chapter 6

Notations

C/C_{tot}	amount of carbon formed during the reduction period over the total amount of carbon introduced during the reduction period *(eq. 2.17)* (-)
H_{CH_4}	lower heating value of methane (MJ/kg)
$k_{\omega,eff}$	effective reaction rate constant *(eq. 2.11)* ($s^{-1}bar^{-1}$)
m	actual mass of oxygen carrier sample in the reactor (g)
m_{bed}	mass of oxygen carrier needed in fuel reactor *(eq. 2.14)* (kg)
m_{ox}	mass of the sample when fully oxidized (g)
m_{red}	mass of the sample in the reduced form (g)
$\dot{m}_O$	stoichiometric mass flow of oxygen to be transferred between two reactors *(eq. 2.15)* (kg/s)
$\dot{m}_{sol}$	oxygen carrier recirculation rate between the air and fuel reactor *(eq. 2.16)* (kg/s)
M_i	molar mass of species i (g/mole)
n_O	moles of oxygen in the oxygen carrier which can be removed from fully oxidized oxygen carrier (mole)
$\dot{n}_{in}$	molar flow of the gas in to the reactor (mole/s)
$\dot{n}_{out}$	molar flow of the gas exiting the reactor after the water has been removed (mole/s)
$p_{CH_4,lgmean}$	log-mean partial pressure of methane (bar)
p_{ref}	reference partial pressure of methane, i.e. 0.15 (bar)
$p_{i,in}$	partial pressure of gas i in to the reactor (bar)
$p_{i,out}$	partial pressure of gas i exiting the reactor after the water has been removed (bar)
p_{tot}	total pressure (bar)

P_{th}	thermal power (MW_{th})
RI	normalized mass-based conversion rate *(eq.2.13)* (%/min)
R_O	Oxygen ratio, i.e. mass ratio between the oxygen which can be removed from fully oxidized oxygen carrier and fully oxidized oxygen carrier. *(eq. 2.8)* (-)
S_r	stoichiometric ratio for reaction between methane and oxygen, i.e. 2 (-)
t	time (s)
X	conversion of oxygen carrier, or the degree of oxidation *(eq. 2.2)* (-)

Greek letters

γ_{red}	gas yield of methane to carbon dioxide (eq. 2.1) (-)
$\Delta\omega$	change of mass-conversion over a cycle (-)
ω	mass-conversion *(eq. 2.7)* (-)
ω_{air}	average mass-conversion in air reactor (-)

Chapter 7

Acknowledgements

I wish to express my sincere gratitude to all the persons who in one way or another contributed to this thesis. In particular, I would like to thank:

My supervisors Professor Anders Lyngfelt and assistant Professor Tobias Mattisson for valuable discussions, experimental suggestions and encouragement.

Professor Oliver Lindqvist for providing me the opportunity to work at the Department of Environmental Inorganic Chemistry at Chalmers University of Technology.

My colleagues Eva Johansson, Marcus Johansson, and Henrik Leion for valuable discussions.

All my colleagues in department, especially my room mates Katarina Gårdfelt and Jonas Sommar.

Marcus Olofsson and Joakim Björnström for all insanities when they were needed the most. Annika Eriksson, Maria Andersson and Amir Ahi should not be forgotten.

Dr. Britt-Marie Steenari for lots of support.

Kajsa Jahrl, Roger Forsberg, Roger Sagdahl, Esa Väänänen, and Charlotte Bouveng for technical and administrative support.

The Swedish Energy Agency is acknowledged for financial support.

Last but not least, I like to thank my family, Julia and our daughter Agnes for their endless support, encouragement and love.

Chapter 8

References

Adánez J, de Diego LF, García-Labiano F, Gayán P, Abad A, **2004a**, Selection of Oxygen Carriers for Chemical-Looping Combustion. Energy & Fuels, 18, 371-377.

Adánez J, García-Labiano F, de Diego LF, Gayán P, Celaya J, Abad A, **2004b**, *Characterization of oxygen carriers for chemical-looping combustion.* Proceedings of the 7th International Conference on Greenhouse Gas Control Technologies, Vancouver, Canada.

Barin I, **1993a**, *Thermochemical Data of Pure Substances, Part I*, VCH Verlags Gesellschaft, Weinheim, Germany.

Barin I, **1993b**, *Thermochemical Data of Pure Substances, Part II*, VCH Verlags Gesellschaft, Weinheim, Germany.

Brandvoll Ø, **2005**, *Chemical-Looping Combustion*. PhD Thesis, NTNU 2005:2, Department of Energy and Process Engineering, Norwegian University of Science and Technology, Trondheim, Norway.

Cho P, Mattisson T, Lyngfelt A, **2002**, *Reactivity of Iron Oxide with Methane in a Laboratory Fluidized Bed - Application of Chemical-Looping Combustion.* Proceedings of the 7th International Conference on Circulating Fluidized Beds, Niagara Falls, Ontario, Canada, 599-606.

Cho P, Mattisson T, Lyngfelt A, **2004**, *Comparison of iron-, nickel-, copper- and manganese-based oxygen carriers for chemical-looping combustion.* Fuel, *83*, 1215-1225.

Cho P, Mattisson T, Lyngfelt A, **2005a**, *Carbon formation on nickel and iron oxide-containing oxygen-carriers for chemical-looping combustion.* Industrial and Engineering Chemistry Research, *44*, 668-676.

Cho P, Mattisson T, Lyngfelt A, **2005b**, *Defluidization Conditions for Fluidized-Bed of Iron, Nickel, and Manganese oxide-Containing Oxygen-Carriers for Chemical-Looping Combustion.* Submitted for publication.

Claridge JB, Green MLH, Tsang SC, York, APE, Ashcroft AT, Battle PD, **1993**, *A study of carbon deposition on catalyst during the partial oxidation of methane to synthesis gas.* Catalysis Letters, 22, 299-305.

de Diego LF, García-Labiano F, Adánez J, Gayán P, Abad A, Corbella BM, Palacios JM, **2004**, *Development of Cu-based oxygen carriers for chemical-looping combustion.* Fuel, 83, 1749-1757.

Copeland RJ, Alptekin G, Cessario M, Gebhard S, Gerhanovich Y, **2000**, *A Novel CO_2 Separation System.* Procdeenings of the 8th International Symposium on Transport Phenomena and Dynamics of Rotating Machinery, Honolulu, Hawaii, USA.

Copeland RJ, Alptekin G, Cessario M, Gerhanovich Y, **2001**, *A Novel CO_2 Separation System.* First National Conference on Carbon Sequestration, National Energy Technology Laboratory (NETL), Washington, USA.

Copeland RJ, Alptekin G, Cessario M, Gerhanovich Y, **2002**, *Sorbent Energy Transfer System (SETS) for CO_2 Separation with High Efficiency.* The 27th International Technical Conference on Coal Utilization & Fuel Systems, Clearwater, Florida, USA.

Corbella BM, de Diego L, García F, Adánez J, Palacios JM, **2005**, *The Performance in a Fixed Reactor of Copper-Based Oxides on Titania as Oxygen Carriers for Chemical Looping Combustion of Methane*, Energy & Fuels, *19*, 433-441.

Couch G, **1994**, *Understanding Slagging and Fouling in Pf Combustion*, Report IEACR/72. IEA Coal Research.

Frenkel M, Kabo GJ, Marsh KN, Roganov GN, Wilhoit RC, **1994a**, *Thermodynamics of organic compounds in the gas state, Vol. 1.*

Frenkel M, Kabo GJ, Marsh KN, Roganov GN, Wilhoit RC, **1994b**, *Thermodynamics of organic compounds in the gas state, Vol. 2.*

García-Labiano F, de Diego LF, Adánez J, Abad A, Gayán, P, **2004**, *Reduction and Oxidation Kinetics of a Copper-Based Oxygen Carrier Prepared by Impregnation for Chemical-Looping Combustion.* Industrial and Engineering Chemistry Research. *43*, 8168-8177.

Hatanaka T, Matsuda S, Hatano H, **1997**, *A New-Concept Gas-Solid Combustion System "MERIT" for High Combustion Efficiency and Low Emissions.* Proceedings of the Intersociety Energy Conversion Engineering Conference, Honolulu, Hawaii, USA, 944-948.

Ishida M, Zheng D, Akehata T, **1987**, *Evaluation of a chemical-looping-combustion power-generation system by graphic exergy analysis*, Energy, *12*, 147-154.

Ishida M, Jin H, **1994a**, *A Novel Combustion Based on Chemical-Looping Reactions and Its Reaction Kinetics.* Journal of Chemical Engineering of Japan, *27*, 296-301.

Ishida M, Jin H, **1994b**, *A new Advanced Power-Generation System Using Chemical-Looping Combustion.* Energy, *19*, 415-422.

Ishida M, Jin H, **1995**, *Chemical-looping combustion power generation plant system.* U.S. Patent 5,447,024.

Ishida M, Jin H, Okamoto T, **1996**, *A Fundamental Study of a New Kind of Medium Material for Chemical-Looping Combustion.* Energy & Fuels, *10*, 958-963.

Ishida M, Jin H, **1996**, *A Novel Chemical-Looping Combustor without NO_x Formation.* Industrial and Engineering Chemistry Research. *35*, 2469-2472.

Ishida M, Jin H, **1997**, *CO_2 Recovery in a Power Plant with Chemical Looping Combustion.* Energy Conversion and Management, *38*, 187-192.

Ishida M, Jin H, Okamoto T, **1998**, *Kinetic Behavior of Solid Particles in Chemical-Looping Combustion: Suppressing Carbon Deposition in Reduction.* Energy & Fuels, *12*, 223-229.

Ishida M, Yamamoto M, Ohba T, **2002**, *Experimental Results of Chemical-Looping Combustion with $NiO/NiAl_2O4$ Particle Circulation at 1200 °C.* Energy Conversion and Management, *43*, 1469-1478.

Jeoung JH, Park JW, Yoon WL, **2003**, *Redox Characteristics of $CoO_x/CoAl_2O_4$ as a Oxygen Carrier for Chemical-Looping Combustion.* Journal of Korean Industrial and Engineering Chemistry, written in Korean, 14, 411-417.

Jin H, Okamoto T, Ishida M, **1998**, *Development of a Novel Chemical-Looping Combustion: Synthesis of a Looping Material with a Double Metal Oxide of CoO-NiO.* Energy & Fuels, *12*, 1272-1277.

Jin H, Okamoto T, Ishida M, **1999**, *Development of a Novel Chemical-Looping Combustion: Synthesis of a Solid Looping Material of $NiO/NiAl_2O_4$.* Industrial and Engineering Chemistry Research, *38*, 126-132.

Jin H, Ishida M, **2001**, *Reactivity Study on Novel Hydrogen Fueled Chemical-Looping Combustion.* International Journal of Hydrogen Energy, *26*, 889-894.

Jin H, Ishida M, **2002**, *Reactivity Study on Natural-Gas-Fueled Chemical-Looping Combustion by a Fixed-Bed Reactor.* Industrial and Engineering Chemistry Research, *41*, 4004-4007.

Johansson E, Mattisson T, Lyngfelt A, Thunman H, **2005**, *A 300 kW laboratory reactor system for chemical-looping combustion with particle circulation,* paper manuscript

Johansson M, **2002**, *Investigation of oxygen carrier materials with TiO_2 support for use in chemical-looping combustion.* MSc Thesis, T2002-263, Department of Energy Conversion, Chalmers University of Technology, Göteborg, Sweden.

Johansson, M., Mattisson, T. and Lyngfelt, A, **2004**, *Investigation of Fe_2O_3 with $MgAl_2O_4$ for chemical-looping combustion.* Industrial and Engineering Chemistry Research, *43*, 6978-6987.

Lee JB, Song YW, Choi SI, Park CS, Kim YH, Yang HS, **2004**, *Characteristics of Redox of Oxygen Carriers with $NiO/AlPO_4$ for Chemical-Looping Combustion.* Journal of Korean Industrial and Engineering Chemistry, written in Korean, 15, 200-204.

Lee JB, Park CS, Choi SI, Song YW, Kim YH, Yang HS, **2005**, *Redox Characteristics of Various Kinds of Oxygen Carriers for Hydrogen Fueled Chemical-Looping Combustion.* Journal of Industrial Engineering Chemistry, *11*, 96-102.

Lyngfelt A, Leckner B, **1999**, *Technologies for CO_2 separation.* Proceedings of the minisymposium on CO_2 capture and storage, Chalmers University of Technology and University of Gothenburg, Göteborg, Sweden.

Lyngfelt A, Leckner B, Mattisson T, **2001**, *A Fluidized-Bed Combustion Process with Inherent CO_2 Separation; Application of Chemical-Looping Combustion.* Chemical Engineering Science, *56*, 3101-3113.

Lyngfelt A, Thunman H, **2005**, *Construction and 100 h of operational experience of a 10-kW chemical looping combustor.* Chapter 36 in Carbon Dioxide Capture for Storage in Deep Geologic Formations - Results from the CO_2 Capture Project, Volume 1 – Capture and Separation of Carbon Dioxide From Combustion Sources. Ed.: Thomas, D. Elsevier Science, London, U.K. 625-646

Mattisson T, Lyngfelt A, Cho P, **2000**, *Possibility of Using Iron Oxide as an Oxygen Carrier for Combustion of Methane with Removal of CO_2 - Application of Chemical-Looping Combustion.* Proceedings of the 5th International Conference on Greenhouse Gas Control Technologies, Cairns, Australia, 205-210.

Mattisson T, Lyngfelt A, **2001**, *Capture of CO_2 Using Chemical-Looping Combustion.* Proceedings of the First Biennial Meeting of Scandinavian-Nordic Section of the Combustion Institute, Göteborg, Sweden, 163-168.

Mattisson T, Lyngfelt A, Cho P, **2001**, *The Use of Iron Oxide as Oxygen Carrier in Chemical-Looping Combustion of Methane with Inherent Separation of CO_2.* Fuel, *80*, 1953-1962.

Mattisson T, Järdnäs A, Lyngfelt A, **2003**, *Reactivity of Some Metal Oxide Supported on Alumina with Alternating Methane and Oxygen - Application for Chemical-Looping Combustion.* Energy & Fuels, *17*, 643-651.

Mattisson T, Johansson M, Lyngfelt A, **2004**, *Multi-Cycle Reduction and Oxidation of Different Types of Iron Oxide Particles -Application of Chemical-Looping Combustion.* Energy & Fuels, 18, 628-637

Mattisson T, Johansson M, Lyngfelt A, **2005** *The use of NiO as an oxygen carrier in chemical-looping combustion.* Submittted for publication.

Nakano Y, Iwamoto S, Maeda T, Ishida M, Akehata T, **1986**, *Characteristics of Reduction and Oxidation Cycle Process by Use of a Fe_2O_3 Medium.* ISIJ International *72*, 1521-1528.

Prieto MdC, Amores JMG, Escribano VS, Busca G, **1994**, *Characterization of Coprecipitated Fe_2O_3-Al_2O_3 Powders.* Journal of Materials Chemistry, *4*, 1123-1130.

Richter HJ, Knoche KF, **1983,** *Reversibility of Combustion Process.* American Chemical Society Symposium Series, Washington D.C., U.S.A., 71-85.

Ryu HJ, Bae DH, Han KH, Lee SY, Jin GT, Choi JH, **2001**, *Oxidation and Reduction Characteristics of Oxygen Carrier Particles and Reaction Kinetics by Unreacted Core Model.* Korean Journal of Chemical Engineering, *18*, 831-837.

Ryu HJ, Bae DH, Jin GT, **2002**, *Carbon Deposition Characteristics of NiO Based Oxygen Carriers Particles for Chemical-Looping Combustor.* Proceedings of the 6th International Conference on Greenhouse Gas Control Technologies, Kyoto, Japan, 175-180.

Ryu HJ, Bae DH, Jin GT, **2003**, *Effect of temperature on reduction reactivity of oxygen carrier particles in a fixed bed chemical-looping combustor.* Korean Journal of Chemical Engineering, *20*, 960-966.

Ryu HJ, Jin GT, Yi CK, Choi JH, **2004**, *Demonstration Of Inherent CO_2 Separation And No Nox Emission In A 50kw Chemical-looping Combustor: Continuous Reduction And Oxidation Experiment,* Proceedings of the 7th International Conference on Greenhouse Gas Control Technologies, Vancouver, Canada.

Song KS, Seo YS, Yoon HK, June CS, **2003**, *Characteristics of the NiO/Hexaaluminate for Chemical-Looping Combustion. Korean Journal of Chemical Engineering, 20*, 471-475.

Villa R, Christiani C, Groppi G, Lietti L, Forzatti P, Cornaro U, Rossini S, **2003**, *Ni Based Mixed Oxide Materials for CH_4 Oxidation under Redox Cycle Conditions.* Journal of Molecular Catalysis A: Chemical, *204-205*, 637-646.

Zafar Q, Mattisson T, Gevert B, **2005**, *Integrated Hydrogen and Power Production with CO_2 Capture using Chemical-Looping Reforming - Redox reactivity of particles of CuO, Mn_2O_3, NiO, Fe_2O_3 using SiO_2 as a support.* Industrial and Engineering Chemistry Research. (in press)